Pluvial periods in Southern Arabia over the last 1.1 million-years

Nicholson, S. L., Pike, A. W. G., Hosfield, R., Roberts, N., Sahy, D., Woodhead, J., Cheng, H., Edwards, R. L., Affolter, S., Leuenberger, M., Burns, S. J., Matter, A. and Fleitmann, D. (2020) Pluvial periods in Southern Arabia over the last 1.1 million-years. Quaternary Science Reviews, 229. 106112. ISSN 0277-3791 doi: https://doi.org/10.1016/j.quascirev.2019.106112 Available at http://centaur.reading.ac.uk/88082/

Samuel L. Nicholson[1], Alistair W.G. Pike[2], Rob Hosfield[1], Nick Roberts[3], Diana Sahy[3], Jon Woodhead[4], Hai Cheng[5,6], R. Lawrence Edwards[5], Stéphane Affolter[7,8,11], Markus Leuenberger[7], Stephen J Burns[9], Albert Matter[10], Dominik Fleitmann[1,11]

[1.] Department of Archaeology, University of Reading, United Kingdom.

[2.] Department of Archaeology, University of Southampton, United Kingdom.

[3.] Geochronology and Tracers Facility, British Geological Survey, Nottingham, United Kingdom.

[4.] School of Earth Sciences, University of Melbourne, Victoria, Australia.

[5.] Department of Earth Sciences, University of Minnesota, Minneapolis, MN, USA.

[6.] Institute of Global Environmental Change, Xi'an Jiaotong University, Xi'an, China

[7.] Physics Institute, University of Bern, Switzerland.

[8.] International Foundation for High Altitude Research Stations Jungfraujoch and Gornergrat, Bern, Switzerland.

[9.] Department of Geosciences, University of Massachusetts, United States of America.

[10.] Institute of Geological Sciences, University of Bern, Switzerland.

[11.] Quaternary Environmental Geology, Department of Environmental Sciences, University of Basel, Switzerland.

Corresponding authors:

Samuel L. Nicholson

s.l.nicholson@pgr.reading.ac.uk

Dominik Fleitmann

dominik.fleitmann@unibas.ch

Department of Archaeology,

Whiteknights Box 227,

Reading,

RG6 6AB,

United Kingdom

Pluvial periods in Southern Arabia over the last 1.1 million-years.

Abstract

Past climates and environments experienced by the Saharo-Arabian desert belt are of prime importance for palaeoclimatic and palaeoanthropological research. On orbital timescales transformations of the desert into a savannah-like landscape in response to higher precipitation provided “windows of opportunity” for hominin dispersal from Africa into Eurasia. On long timescales, palaeoenvironmental reconstructions for the region are predominantly derived from marine sediments and available terrestrial records from the Arabian Peninsula are limited to 450 ka before present (BP). Here, we present a new stalagmite-based palaeoclimate record from Mukalla Cave in

Yemen which extends back to ~1.1 million years BP or Marine Isotope Stage (MIS) 31, as determined by Uranium-lead dating. Stalagmite Y99 grew only during peak interglacial periods and warm substages back to ~1.1 Ma. Stalagmite calcite oxygen isotope ($\delta^{18}O$) values show that every past interglacial humid period was wetter than the Holocene, a period in which large lakes formed in the now arid areas of southern Arabia. Carbon isotope ($\delta^{13}C$) values indicate habitable savannah-like environments developed during these pluvial periods. A total of 21 pluvial periods with precipitation of more than 300 mm yr^{-1} occurred since ~1.1 Ma and thus numerous opportunities for hominin dispersals occurred throughout the Pleistocene. New determinations of hydrogen (δD_{FI}) and oxygen ($\delta^{18}O_{FI}$) isotopes in stalagmite fluid inclusion water demonstrates that enhanced precipitation in Southern Arabia was brought by the African and Indian Summer Monsoons. When combined with sub-annual calcite analysis of $\delta^{18}O$ and $\delta^{13}C$, these data reveal a distinct wet (summer) and dry (winter) seasonality.

Highlights

- Pluvial periods recorded in stalagmites from Southern Arabia up to 1.073 Ma (MIS 31)
- Speleothem growth in Yemen only occurred during interglacial maxima and warm substages
- The African Summer Monsoon (ASM) and Indian Summer Monsoon (ISM) increased precipitation to Southwestern Arabia
- Monsoonal rainfall increased precipitation to south-eastern Arabia
- All Pleistocene pluvial periods were wetter than the Holocene pluvial period
- Grassland environments formed during peak interglacials
- Interglacial grasslands provided “windows of opportunity” for hominin occupation of the now arid Arabian interior and dispersals from Africa.

Keywords

Human dispersal, Middle East, Pleistocene, Speleothems, Arabia, Oxygen-isotopes, Carbon-isotopes, Water-isotopes, Uranium-series dating, Monsoon.

1. Introduction

The Saharo-Arabian desert belt is a key-area for both palaeoclimatic and palaeoanthropological research. On orbital timescales, changes in the intensity and spatial extent of the African (ASM) and Indian Summer monsoons (ISM) transformed the Saharo-Arabian desert belt into a "green" landscape with abundant lakes (Drake et al., 2011; Fleitmann et al., 2011; Rosenberg et al., 2011, 2012, 2013; Bretzke et al., 2013; Larrasoaña et al., 2013; Matter et al., 2015; Breeze et al., 2016; Drake and Breeze, 2016). The timing and duration of these humid periods were pivotal "windows of opportunity" for hominin dispersals from Africa into Eurasia ("out-of-Africa"), which caused substantial demographic shifts during the last 130 ka (Timmermann and Friedrich, 2016; Bae et al., 2017). Knowledge of the "permeability" of the Saharo-Arabian desert belt on longer timescales could therefore be linked to potentially earlier hominin dispersals (e.g., Hershkovitz et al., 2018; Harvati et al., 2019). To date, two dispersals routes into Eurasia are favoured, the Levantine corridor (the *northern route*) and the narrow strait of Bab-al-Mandab (the *southern route*) (Fernandes et al., 2006; Fleitmann et al., 2011; Lambeck et al., 2011; Grant et al., 2012; Rohling et al., 2013; Breeze et al., 2016).

Marine sediments from the Mediterranean (ODP 967, Larrasoana et al., 2003; Grant et al., 2017), the Red Sea (KL 11, Fleitmann, 1997) Gulf of Aden (KL 15, Fleitmann, 1997; RC09-166, Tierney et al., 2017) and Arabian Sea (ODP 721/722, deMenocal, 1995; Clemens and Prell, 2003) provide long and continuous records of climate changes in the Saharo-Arabian desert belt, with a few extending back to the Pliocene. The majority of these records use terrigenous dust as a proxy for continental wetness, where reduced dust input and grain size data are related to enhanced vegetation cover during periods of higher precipitation (Fleitmann, 1997; Larrasoana et al., 2003). However, mobilisation, transport and deposition of dust is determined by multiple non-linear factors, such as production of dust,

92 transport paths (wind direction), wind strength, erosion and vegetation density (Zabel et al., 2001).
93 Terrestrial archives are thus required to test and mitigate uncertainties within marine dust records.

94 Terrestrial records from the main dispersal routes (Fig. 1) are primarily based on lacustrine sediments
95 and speleothems (Burns et al., 2001; Armitage et al., 2007; Vaks et al., 2010; Fleitmann et al., 2011;
96 Petraglia et al., 2011; Rosenberg et al., 2011, 2012, 2013; Jennings et al., 2015b), which cover only the
97 last 350 to 450 ka before present (BP) (Rosenberg et al., 2013; Parton et al., 2018). While lake records
98 provide information on the timing of these pluvial periods, it is much more difficult to use them for
99 characterizing the climatic conditions at the time of their formation (Rosenberg et al., 2011, 2012,
100 2013). Palaeolake formations currently only provide limited “wet” or “dry” environmental
101 information; comparison of climates among interglacial periods is much more challenging. Moreover,
102 the nature of the lakes is the subject of debate, i.e. whether seasonal "wetlands" or perennial lakes
103 existed (Enzel et al., 2015; Engel et al., 2017; Quade et al., 2018). Furthermore, palaeolake records
104 from Arabia cannot currently be used to determine the source of moisture; a contentious issue within
105 palaeoclimate research (Fleitmann et al., 2003b; Rosenberg et al., 2013; Kutzbach et al., 2014;
106 Jennings et al., 2015b; Torfstein et al., 2015). Thus, an independent archive of continental wetness is
107 required to elucidate these issues.

108 Speleothems (stalagmites, stalactites and flowstones) from the Arabian Peninsula and Middle East
109 have great potential to deliver more comprehensive climatic records as they are protected from
110 erosion. In addition, they can be used to extend the terrestrial palaeoclimate record beyond 600 ka
111 using the Uranium-Lead (U-Pb hereafter) chronometer (Woodhead et al., 2006, 2012; Vaks et al.,
112 2013, 2018). In arid regions such as Arabia, speleothem growth is dependent on both availability of
113 moisture and vegetation respired CO_2 in soils (Burns et al., 1998; McDermott, 2004). The amount and
114 source of precipitation are important controls on speleothem calcite $\delta^{18}O_{ca}$ values (Dansgaard, 1964;
115 Fleitmann et al., 2003a, 2011); whereas carbon isotopes ($\delta^{13}C_{ca}$) can provide information on the type
116 (C_3/C_4 plants) and density of vegetation above the cave (McDermott, 2004; Cerling et al., 2011; Rowe

et al., 2012). Finally, δD_{FI} and $\delta^{18}O_{FI}$ values of water trapped in speleothem fluid inclusion provide direct evidence of moisture sources when compared to modern isotopes in precipitation and regional meteoric waterlines (Bar-Matthews et al., 1996; Dennis et al., 2001; Meckler et al., 2015).

Previously published stalagmite records from Mukalla Cave in Yemen and Hoti Cave in Northern Oman (Fig. 1) extend back to ~330-300 ka BP, or Marine Isotope Stage (MIS) 9 (Fleitmann et al., 2011). The unique geographical position of Mukalla cave means speleothem growth occurs only when the northern limit of the monsoon rain belt passes ~14°N. Stalagmite Y99 (Mukalla Cave) is therefore an ideal specimen to track both meridional and zonal movements of the monsoon rain belt in southern Arabia and eastern Africa. Here, we present new Uranium-Thorium (^{230}Th) and Uranium-Lead (U-Pb) dates for stalagmite Y99, which allows us to expand the Arabia terrestrial palaeoclimate record back to ~1.073 Ma, or MIS 31. Additional isotope measurements performed on Mukalla and Hoti Cave stalagmite calcite and fluid inclusion water allow us to track changes in the amount and source of rainfall.

2. Climatic and Cave settings

Stalagmites presented in this study were collected from Mukalla Cave in Yemen and Hoti Cave in Northern Oman (Burns et al., 2001; Fleitmann et al., 2003b, 2011). Present-day climate in Southern Arabia is strongly governed by two major weather systems: The North Atlantic/Siberian pressure system in winter/spring and the ASM/ISM in summer (Fleitmann et al., 2003b). At present, hyper-arid to arid climate conditions prevail on the Arabian Peninsula and only the southernmost parts, such as the Yemen Highlands and Dhofar Mountains, are affected by the ASM and ISM.

2.1 Mukalla Cave, Yemen

Mukalla Cave (14°55'02''N; 48°35'23'' E; ~ 1500 metres above sea level, masl) is situated in the arid desert of Yemen, approximately 70 km North of Al Mukalla, Hadhramaut (Fig. 1). The current climate of Southern Yemen is dependent on the annual northward movement of the Intertropical

Convergence Zone (ITCZ) and associated monsoonal rainfall belt. Annual precipitation is highly variable, yet averages ~120 mm yr^{-1}, mostly delivered in the spring and summer months (Mitchell and Jones, 2005). Bedrock thickness above the cave is approximately 30 m, and soil above the cave is mostly absent. No actively growing stalagmites were found when stalagmites Y99, Y97-4 and Y97-5 were collected in 1997 and 1999 respectively (Fleitmann et al., 2011), indicating that modern rainfall is too low to recharge the aquifer above Mukalla Cave. Based on these samples, Fleitmann et al. (2011) produced an environmental record up to MIS 9 (~330 ka), identifying four distinct growth intervals (GI I-IV) within stalagmite Y99. However, only the top section (collected in whole; Fig. 2B and S1) of a 3.2m sample (Y99) was analysed. Here, remaining growth intervals from the lower part of Y99 (which was cored in several overlapping sections; Fig. 2C, S2 and S3), was dated to expand the terrestrial palaeoclimate record of Arabia. Calcite isotope measurements were performed throughout these growth intervals to characterise the climatic and environmental conditions during stalagmite growth. Additional calcite isotope measurements were performed at greater resolution in the top section of Y99.

2.2 Hoti Cave, Oman

Hoti Cave (23°05'N; 57°21'E: ~ 800 masl, Fig. 1) is located in the northern Oman mountains, where annual precipitation ranges between 50 and 255 mm yr^{-1} (station Al Hamra, 700 masl, 1974–1997). Precipitation is highly variable and mainly derived from three sources: the Mediterranean frontal system (December-March: Weyhenmeyer et al., 2002); orographic rain produced over the Jabal Akhdar Mountains during summer; and tropical cyclones, originating in the south-eastern Arabian Sea and the Bay of Bengal, every 5 to 10 years (Pedgley, 1969).

Stalagmites from Hoti Cave have been extensively studied (Burns et al., 2001; Neff et al., 2001; Fleitmann et al., 2003b, 2007). Several stalagmites cover the Holocene (samples H5, H12 and H14) and beyond (samples H1, H4, and H13). Stalagmite H13 is a ~3 m tall stalagmite covering MIS 5e, MIS 7e

and MIS 9. Further details on the chronology and sampling location of Hoti Cave were presented in previous publications (Burns et al., 1998, 2001; Neff et al., 2001; Fleitmann et al., 2003b, 2007, 2011).

3 Methods

3.1 Dating

Stalagmites presented in this study were dated using the ^{230}Th dating method back to ~550 ka and the U-Pb method for older samples (Woodhead et al., 2006; Cheng et al., 2013). The ^{230}Th ages for Hoti Cave stalagmites are reported in Fleitmann et al. (2007, 2003a). For stalagmite Y99 (Mukalla Cave), a total of seventy ^{230}Th ages were determined back to approx. 550 ka BP (Tab. S1-S3). Nineteen samples were analysed at the University of Minnesota (following the methods outlined by Cheng et al., 2013) and twelve additional samples were analysed at the British Geological Survey, Nottingham, UK (following the methods outlined by Crémière et al., 2016). Dates were calculated using the decay constant of Cheng et al. (2013), and a correction for the presence of initial ^{230}Th was applied assuming a detrital U-Th isotope composition of (^{232}Th/^{238}U) = 1.2 ± 0.6, (^{230}Th/^{238}U) = 1 ± 0.5 and (^{234}U/^{238}U) = 1 ± 0.5. The ages for GI XII and GI XVIII were determined via U-Pb methods. U-Pb ages for the lower part of Y99 were produced using both traditional solution-mode multi-collector inductively coupled plasma mass spectrometry (MC-ICP-MS) (following the methods detailed in: Woodhead et al., 2006) analysis (University of Melbourne, Australia) along with the recently developed Laser ablation (LA) method (BGS) (Tab. S4 and S5). For LA-ICP-MS, the methods and analytical protocol follows that described by Coogan et al. (2016); U/Pb ratios were normalised to WC-1 carbonate (Roberts et al., 2017) and Duff Brown carbonate (Hill et al., 2016) was run as a check on accuracy.

3.2 Calcite oxygen and carbon isotope analysis

A total of 910 samples were collected along the main growth axes of stalagmite Y99 GIs for stable isotope analysis. Samples were collected at resolutions of ~1mm for growth phase I and II, ~2 mm for growth phases III-VII and ~5 mm for growth phases VII-XVIII (Tab. S6). Due to the variable size, visibility

and direction of independent growth layers, it was not possible to produce Hendy tests. To provide addition support for our Growth Interval assignments, additional samples were collected across visible growth discontinuities at 1 mm resolution within the lower sections of Y99 (Tab. S7; Fig. 2). Furthermore, H13 (Hoti Cave) was selected for sub-annual isotopic analysis to examine seasonality, due to its annual laminations. Samples were collected at 0.1mm resolution (Tab. S8).

Isotope measurements were performed using a Finnigan Delta V Advantage Isotope Mass Spectrometer (IRMS) coupled to an automated carbonate preparation system (Gasbench II). Precision (1σ) is ≤0.2‰ for $\delta^{18}O$ and ≤0.1‰ for $\delta^{13}C$. Measurements were performed at the Chemical Analysis Facility (CAF), University of Reading, UK, and the Institute of Geological Sciences, University of Bern, Switzerland. Isotope values are reported relative to the Vienna Peedee Belemnite (VPDB) standard.

3.3 Fluid inclusion deuterium and oxygen isotope analysis

Deuterium (δD_{FI}) and oxygen ($\delta^{18}O_{FI}$) isotopes of speleothem fluid inclusion water were analysed at the Physics Institute, University of Bern, Switzerland, using a recently developed extraction method (Affolter et al., 2014, 2015). Sixteen calcite blocks of ~25 x 5 x 5 mm (L, W, H) for fluid inclusion analysis were collected from Y99, H13 and H5. Samples were placed into a copper tube and connected to the measuring line, heated to ~140°C and crushed, the liberated water was then transported to a wavelength scanned cavity ring down spectroscopy system (Picarro L2401-i analyser) under humid conditions (with standardised water of known isotopic composition) to prevent fractionation and minimize memory effects. The crushing of samples released, on average, ~1 µl of water. Precision is 1‰ for δD_{FI} and 0.2‰ for $\delta^{18}O_{FI}$. Fluid inclusion values are reported on the Vienna Standard Mean Ocean Water (V-SMOW) scale (Tab. S9).

4. Results and Discussion

This section is divided into two parts. In the first part we focus on rainfall variability during the last 350 ka. We provide additional and more precise ^{230}Th ages for Y99 (Mukalla Cave), as well as stable

isotope analysis of calcite and fluid inclusion water from Y99 (Mukalla Cave), H5 and H13 (Hoti Cave). We combine these ages with previously published Mukalla and Hoti Cave speleothem data to discuss the timing and environmental conditions of South Arabian Humid Periods (SAHPs) since 350 ka BP. By comparing our multiproxy records with marine and terrestrial palaeoclimate records from the African and Asian monsoon domains, we show that periods of enhanced rainfall and speleothem growth in Southern Arabia are related to a strengthening and greater spatial extent of the ASM and ISM during peak interglacials and interstadials. Within the second section, we provide an extended chronology and $\delta^{18}O_{ca}$ and $\delta^{13}C_{ca}$ stable isotope data for the lower portion of Y99 (Fig. 2C) in order to characterise humid periods in Southern Arabia back to ~1.1 Ma BP, making the stalagmite Y99 record one of the longest continental records from Southern Arabia.

4.1 Timing and Nature of SAHPs during the last 350 ka

4.1.1 Chronology of Y99 GI I to V

The chronology of Y99 growth phase I to V is based on a total of 53 ^{230}Th ages (Fig. 3). These include 38 ages presented in Fleitmann et al. (2011) and 15 additional more precise ^{230}Th ages analysed for this study (Tab. S1 and S2). Stalagmite Y99 GIs I-V coincide with peak interglacial periods and interstadials corresponding to MIS 5e, 7a, 7e, 9c and 9e (Fig. 4) when Southern Arabia was affected by the ASM and ISM (Fleitmann et al., 2011; Rosenberg et al., 2013). While age reversals are observed in GI IV and V, kernel probability density plots of all ^{230}Th ages obtained from Mukalla Cave (Y99, Y97-4.-5) and Hoti Cave (H1, H4, H5, H10, H11 and H14) indicates Y99 growth was more likely to occur within MIS 9c and 9e (Fig. 3).

4.1.2 SAHPs in Oman and Yemen during the last 350 ka

Growth intervals of stalagmites from Mukalla and Hoti Caves mark climatic intervals when effective precipitation was high enough to recharge the aquifers above both caves (Burns et al., 2001; Fleitmann et al., 2003b, 2011; Fleitmann and Matter, 2009). At present, total annual rainfall averages ~120 mm

237 yr^{-1} and ~180 mm yr^{-1} at Mukalla and Hoti Cave respectively, and actively growing stalagmites are
238 either absent (Mukalla Cave) or very rare (Hoti Cave) (Burns et al., 2001; Fleitmann et al., 2003a, 2007,
239 2011). Thus, the existence of very tall and large diameter stalagmites such as H13 and Y99 (Fig. 2) in
240 both caves is clear evidence that precipitation was considerably higher than today when they were
241 formed (Vaks et al., 2010; Fleitmann et al., 2011; El-Shenawy et al., 2018). Based on the spatial
242 distribution of actively growing stalagmites in the Levant and Negev – areas with very similar climatic
243 conditions compared to Yemen and Oman – precipitation should have been around 300 mm yr^{-1} or
244 greater to recharge the groundwater and trigger growth of stalagmites (Vaks et al., 2010, 2013).
245 Considering the height and diameter of stalagmites Y99 and H13 (Fig. 2), precipitation was most likely
246 considerably higher than 300 mm yr^{-1}. Intervals of speleothem growth at both cave sites are therefore
247 a first indicator for continental wetness in Southern Arabia. An important feature of stalagmites Y99
248 and H13 is that their growth was reactivated multiple times, suggesting that the long-lasting cessations
249 of stalagmite growth are related to arid climatic conditions (Burns et al., 2001; Fleitmann et al., 2011).

250 Over the last 350 ka BP, stalagmite growth in Mukalla and Hoti Caves (Fig. 4) occurred during peak
251 interglacial periods and warmer substages corresponding to the early and mid-Holocene, MISs 5a, 5c,
252 5e, 7a, 7e, 9c and 9e (Fig. 4; Burns et al., 2001; Fleitmann et al., 2003a, 2003b; 2011; Fleitmann and
253 Matter, 2009). SAHPs were related to intensified African and Indian summer monsoon circulation and
254 a northward displacement of the tropical rain-belt and ITCZ at times of high boreal summer insolation
255 and low ice volume (LR04 stack) (Burns et al., 1998, 2001; Fleitmann et al., 2011; Beck et al., 2018).
256 Both the timing and frequency of SHAPs over the last 350 ka are in excellent agreement with other
257 marine and terrestrial hydroclimate records from the Saharo-Arabian desert belt (Fig. 4). In the Gulf
258 of Aden, low $\delta D_{leafwax}$ values in Core RC09-166 (Fig. 4) indicate greater rainfall in the Horn of Africa and
259 Afar regions during the early to mid-Holocene (SAHP 1), MIS 5a, 5c, 5e (SAHPs 2-4) and MIS 7a (SAHP
260 5) (Tierney et al., 2017). Two aeolian dust records from the Gulf of Aden (KL 15) and central Red Sea
261 (KL 11) show generally lower median grain size values during peak interglacial periods when erosion
262 and mobilization of dust was significantly reduced as a result of a denser vegetation cover in North

Africa and Arabia (Fleitmann, 1997). Similarly, speleothem growth in Southern Arabia and Northern Egypt (Wadi Sannur Cave) are in good agreement, occurring at MIS 5e, MIS 7c and MIS 9c and 9e (El-Shenawy et al., 2018). Absence of speleothem growth in Northern Egypt during relatively warm substages (MIS 5c and 5a and MIS 3) suggests that ASM rainfall did not reach far into Egypt, highlighting a degree of regional and temporal variability. Sapropel layers in the Eastern Mediterranean are an additional proxy for ASM and ISM intensity and were mainly deposited during periods of increased Mediterranean rainfall and significantly higher monsoon precipitation in the Ethiopian highlands and resultant higher Nile discharge (Fig. 4; summarized in Rohling et al., 2015; Grant et al. 2016). The timing of SAHPs 1 to 8 is in excellent agreement with sapropels records, with the exception of the "ghost sapropels" 2 and 6 which are most likely not associated with higher Nile discharge (Rohling et al., 2015). Further north, the Soreq and Peqiin Cave $\delta^{18}O_{ca}$ records from the Levant are also sensitive recorders of changes in $\delta^{18}O$ of eastern Mediterranean surface seawater related to Nile discharge (Bar-Matthews et al., 2003; Rohling et al., 2015), with more negative $\delta^{18}O_{ca}$ values indicating higher Nile discharge during peak interglacial and interstadial periods (Fig. 4). Likewise, speleothem-based Negev Humid Periods (NHPs; based on speleothem ages) 1-4 are synchronous to SAHPs (Fig. 4), with the exemption of SAHP 6 (~245-241 ka), in which there is only limited evidence of speleothem deposition (Vaks et al., 2010). Also, SAHPs 1-8 correlate to phases of lake formation in the Nafud desert in Northern Arabia related to enhanced ASM rainfall (Rosenberg et al., 2013; Jennings et al., 2015b). SAHPs are therefore in phase with wet intervals in Northern Arabia. One notable discrepancy, however, is the lack of evidence for stalagmite growth in Mukalla and Hoti Caves during MIS 7c (Fig. 4); whereas increased precipitation is observed in Wadi-Sannur Cave, Peqiin and Soreq $\delta^{18}O_{ca}$ records, KL-15 grain size and Mediterranean sapropels (S8) (Fig. 4). MIS 7c is also reflected by a less substantial enhancement of the monsoon in Asia (Beck et al., 2018) and KL-11 (Fleitmann et al., 1997) (Fig. 4). The reason of lack of evidence for an SAHP during MIS 7c remains unknown. Furthermore, we acknowledge that some fluvio-lacustrine deposition and alluvial aggradation occurred in Arabia during MIS 6 and 3 (e.g., McLaren et al., 2009; Parton et al., 2013,

289 2015, 2018; Hoffmann et al., 2015). Previous analyses have shown that that only 200 mm yr^{-1} is
290 required to activate alluvial systems in Arabia (Parton et al., 2015); whereas more than 300 mm yr^{-1}
291 required to active the growth of tall stalagmites (Vaks et al., 2010; Fleitmann et al., 2011).

292 The influence of precessional and glacial boundary forcing on Asian monsoon intensity remains
293 controversial, as some monsoon records suggest dominant precession-driven monsoon maxima
294 during Northern hemisphere summer insolation maxima (Cheng et al., 2016) while others show
295 evidence for a dampening effect of glacial boundary conditions on monsoon strength during glacial
296 periods (Burns et al., 2001; Fleitmann et al., 2003a; Beck et al., 2018). A recently published East Asian
297 summer monsoon (EASM) reconstruction based on ^{10}Be-flux from Chinese loess shows highest
298 summer monsoon rainfall during peak interglacial periods (Fig. 4). The ^{10}Be-flux rainfall EASM record
299 is closely linked with global ice volume, which is consistent with the timing of SAHPs 1-8 in our
300 speleothem record (Fig. 4).

301 In summary, there is excellent agreement between SAHPs and low latitude northern-hemisphere
302 insolation, glacial boundary conditions and African and Asian (Indian) monsoon records. This adds
303 confidence that the Mukalla and Hoti Cave speleothems are an accurate recorder of changes in ASM
304 and ISM intensity and extent in north-eastern Africa and Southern Arabian Peninsula.

305 *4.1.3 Source of moisture in Southern Arabia during SAHPs 1 to 8*

306 Current climate reconstructions derived from lacustrine sediments and dune deposits are unable to
307 identify the source of precipitation during Arabian pluvial periods (Fleitmann et al., 2003b; Kutzbach
308 et al., 2014; Enzel et al., 2015; Torfstein et al., 2015; Engel et al., 2017). This has triggered controversial
309 debates about the origin of rainfall at the time of their formations. Enzel et al. (2015), for instance,
310 questioned the paradigm that enhanced precipitation in Arabia was related to an amplification of the
311 ASM and ISM and northward displacement of the summer ITCZ. Instead, Enzel et al. (2015) proposed
312 two other potential sources of precipitation in Oman during the early and mid-Holocene humid period
313 (SAHP 1): more frequent Arabian Sea cyclones or enhanced advection of moisture from the Gulf of

Oman in winter. Direct measurements of hydrogen and oxygen isotope values in speleothem fluid inclusions from Hoti and Mukalla Caves provide direct information on drip water isotopic composition and palaeoprecipitation respectively (Fleitmann et al., 2003b). Stalagmite δD_{FI} and $\delta^{18}O_{FI}$ values enable us to determine the origin (e.g., Mediterranean or Indian Ocean) and transport of moisture to Southern Arabia during pluvial periods. Furthermore, they also permit a direct comparison with isotope-enabled climate model simulations, to benchmark the models (Herold and Lohmann, 2009) and also help to settle current debates about the origin and seasonality of precipitation in Southern Arabia.

At present, a large proportion of moisture in Yemen derives from the northern reach of the ISM (Fleitmann et al., 2011) with additional moisture originating from Africa (by the ASM) and the Red Sea (mainly in winter/spring) (e.g., Al-ameri et al., 2014). The isotopic composition of modern precipitation (collected between 2008 and 2010) from sampling sites between 500 and 1700 meters asl in Yemen ranges from around -40 to 40‰ and -4 to 8‰ in δD and $\delta^{18}O$ respectively, and rainfall plots along the Global Meteoric Waterline (GMWL; $\delta D = 8\ \delta^{18}O + 10$; Fig. 5A; Al-ameri et al., 2014). In contrast, stalagmite Y99 fluid inclusion isotope values for MISs 5e (SAHP 4) and 7e (SAHP 6) are more negative and range from -64.5‰ to -35.0% and -8.6 and -4.5‰ in δD and $\delta^{18}O$ respectively (Fig. 5A; Tab. S9). Like modern rainfall, Y99 fluid inclusion isotope values plot close to the GMWL, whereas some samples appear to be slightly affected by evaporation as they plot below the GMWL. Stalagmite Y99 MIS 5e and MIS 7e δD_{FI} and $\delta^{18}O_{FI}$ values are more negative than isotope values in modern summer monsoonal rainfall (June to September) in Addis Ababa, Ethiopia, where moisture is delivered by the African and Indian summer monsoons. This suggests that enhanced rainfall at Mukalla Cave during MIS 5e (SAHP 4) and MIS 7e (SAHP 6) resulted from an amplification of the ASM and/or ISM (Fig. 5C). Our assumption is also supported by climate model data for MIS 5e (Herold and Lohmann, 2009; Jennings et al., 2015b), which indicate a more zonal transport of moisture from Africa to the Arabian Peninsula during MIS 5e (SAHP 4). Y99 $\delta^{18}O_{FI}$ values of around -7.2 ± 1.5‰ during MIS 5e are within the range of modelled summer precipitation $\delta^{18}O$ values of between -6 and -7‰ in Yemen (Fig. 5C).

Finally, significant contributions of rainfall from a Mediterranean source can be excluded as Y99 δD_{FI} and $\delta^{18}O_{FI}$ values plot below the Mediterranean Meteoric Waterline (MMWL; $\delta D = \delta^{18}O + 22$; Fig. 5A).

In Northern Oman, present-day rainfall originates predominantly from a northern (Mediterranean) and a southern (Indian Ocean) moisture source. As a result, two distinctly different local meteoric waterlines exist, the Northern Meteoric Waterline (N-LMWL; $\delta D = 5.0\ \delta^{18}O + 10.7$) and the Southern Local Meteoric Waterline (S-LMWL; $\delta D = 7.1\ \delta^{18}O - 1.1$) (Fig. 5B; Weyhenmeyer et al., 2002; Fleitmann et al., 2003b). Precipitation originating from a northern moisture source ranges from -4.5 to 1.0‰ in $\delta^{18}O$ and from -25 to 5‰ in δD, whereas precipitation from a southern moisture source is more negative, with $\delta^{18}O$ values varying from -10 to -2‰ and δD values from -75 to -15‰ (Weyhenmeyer et al., 2002; Fleitmann et al., 2003b). Modern groundwater in Northern Oman (N-OGL: $\delta D = 5.3\ \delta^{18}O + 2.7$) and cave drip water in Hoti Cave is intermediate between both sources, indicating that both contribute to groundwater recharge (Weyhenmeyer et al., 2002; Fleitmann et al., 2003b; Fig. 5B). The isotopic composition of fluid inclusion water extracted from the Holocene stalagmite H5 (SAHP 1: 10.9 ka-6.2 ka; Neff et al., 2001; Fleitmann et al., 2007) ranges from -21.4‰ to -13.2‰ in δD_{FI}, and -3.2‰ to -0.7‰ in $\delta^{18}O_{FI}$. Fluid inclusion water extracted from the MIS 5e (SAHP 4) section of stalagmite H13 is more negative and measured -41.7‰ for δD_{FI} and -7.8‰ to -4.2‰ for $\delta^{18}O_{FI}$. Both H5 and H13 fluid inclusion values plot closer to the S-OMWL (Fig. 5B), indicating the ISM was the primary moisture source in Oman during peak interglacials (Fleitmann et al., 2003b). One sample, however, plots above the S-OMWL, yet this remains more closely aligned to modern southern groundwater values. Overall, Hoti Cave δD_{FI} and $\delta^{18}O_{FI}$ values show clear evidence that enhanced rainfall during the early to middle Holocene (SAHP 1) and MIS 5e (SAHP 4) was related to an intensification of the ISM. This is in stark contrast to suggestions that enhanced frontal depressions from the Persian Gulf and/or Mediterranean increased precipitation during the early to mid-Holocene wet period (SAHP 1) (Enzel et al., 2015).

When compared to isotope-enabled climate model simulation, the measured isotope $\delta^{18}O_{FI}$ values at both caves for SAHP 4 (MIS 5e) are in good agreement with modelled $\delta^{18}O$ of summer precipitation (Fig. 5C). Furthermore, the distinct isotopic gradient across Southern Arabia is also supported by the Y99 and H13 $\delta^{18}O_{FI}$ values, with more negative modelled summer rainfall $\delta^{18}O$ values prevailing in the west due to a greater moisture supply from the African summer monsoon (Herold and Lohmann, 2009). Thus, growth intervals and isotope values in stalagmites from Mukalla Cave are excellent proxies for the intensity of the ASM in eastern Africa, whereas stalagmites from Hoti Cave are more closely connected to intensity changes of the ISM and, to a lesser extent, ASM. This is also in agreement with climate model simulations for MIS 5e, which indicate that higher precipitation in Northern Oman was associated with the ASM and ISM, with negligible and fairly stable contribution of rainfall from Mediterranean westerlies (Jennings et al., 2015b).

4.1.4 Comparison between pluvial conditions in Southern Arabia during the last 350 ka

$\delta^{18}O_{ca}$ values of stalagmites from Southern Arabia are primarily controlled by two effects: i.e. the amount and source of rainfall (Fleitmann et al., 2003b, 2004, 2007, 2011). $\delta^{18}O_{ca}$ values of Mukalla Cave stalagmites are generally more negative than those of stalagmites from Hoti Cave (Fig. 6A), with a west-east (Mukalla-Hoti) isotopic gradient of between 2 and 4 ‰ during SAHPs 1-7. This gradient is also evident in δD_{FI} and $\delta^{18}O_{FI}$ values from both caves and in simulated MIS 5e $\delta^{18}O$ in summer precipitation across Southern Arabia (Fig. 6A). This adds further confidence in the palaeoclimatic significance of $\delta^{18}O_{ca}$ values from Mukalla and Hoti Caves. Furthermore, $\delta^{18}O_{ca}$ values from both cave sites reveals marked and consistent differences in the amount of rainfall between among the SAHPs (Fig. 8). The most striking feature of the Mukalla and Hoti Cave records is the fact that least negative $\delta^{18}O_{ca}$ values were obtained from early to mid-Holocene stalagmites, indicating that monsoon rainfall during SAHP 1 was the lowest in the last 350 ka. On the other hand, monsoon precipitation was highest at both caves during SAHP 4 (MIS 5e). When we combine our fluid inclusion data with the relatively consistent $\delta^{18}O_{ca}$ between SAHPs, we can show that the moisture source was likely consistent

389 throughout SAHPs. Modern $\delta^{18}O_{ca}$ values from Hoti Cave (derived from the winter Mediterranean
390 precipitation source) are more positive than SAHP values (Fig. 6A). SAHP 1 (early to middle Holocene),
391 4 (MIS 5e) and 6 (MIS 7e) FI data allows us to confidently state that $\delta^{18}O_{ca}$ of these periods represents
392 a monsoon rainfall signature. Thus, we can use the more positive $\delta^{18}O_{ca}$ values (Mediterranean
393 signature) of modern and more negative $\delta^{18}O_{ca}$ values (monsoon signature) of past precipitation to
394 posit that monsoon precipitation was the dominant source of preceding SAHPs. This isotopic
395 relationship has also been observed in previously published high-resolution $\delta^{18}O_{ca}$ profiles of H5 and
396 H12 (Fig. 6B), where an abrupt shift from more negative values (increased precipitation from the ISM)
397 to more positive values (reduced precipitation delivered by Winter Mediterranean Cyclones (WMCs))
398 occurred at the termination of the early Holocene pluvial period (SAHP 1) (Fleitmann et al., 2007).

399 *4.1.5 Environmental conditions*

400 Mukalla Cave speleothem $\delta^{13}C_{ca}$ values vary between -8 and 2‰ (VPDB) (Fig. 7; Tab. S11). Such a wide
401 range in $\delta^{13}C_{ca}$ is quite common in speleothems as $\delta^{13}C_{ca}$ depends on a variety of environmental, partly
402 counteracting, parameters, including: (1) type and density of vegetation, (2) soil thickness and
403 moisture, (3) biological activity within the soil, (4) recharge conditions and (5) kinetic isotope
404 fractionation during calcite precipitation, the latter factor is influenced by cave air PCO_2 and drip rate
405 (e.g., Baker et al., 1997). At times of high precipitation and short soil-water residence times,
406 equilibration between soil CO_2 and percolating water may be incomplete. Under such a scenario,
407 seepage water would have a stronger atmospheric CO_2 component and thus speleothem $\delta^{13}C_{ca}$ values
408 would be more positive. In addition, CO_2 degassing within the cave can lead to more positive
409 speleothem $\delta^{13}C_{ca}$ values and thus blur the biogenic signal. Overall, speleothem $\delta^{13}C_{ca}$ values can be
410 difficult to interpret, which is one reason why the Hoti Cave $\delta^{13}C_{ca}$ records were never used for
411 palaeoenvironmental reconstructions. This is also related to the fact that Hoti Cave has two entrances
412 and therefore strong ventilation, leading to fluctuations in cave air PCO_2 and strong kinetic
413 fractionation of $\delta^{13}C$ during calcite precipitation. In contrast, Mukalla Cave has only one narrow

entrance and ventilation within the cave is therefore low. Mukalla Cave stalagmite $\delta^{13}C_{ca}$ values are therefore more closely related to surface vegetation and biological soil activity, provided that complete equilibration ("open system conditions") between soil CO_2 and soil water has occurred. Under such conditions, $\delta^{13}C_{ca}$ values of a stalagmite growing under a C_3 plant dominated environment vary between -14 and -6‰ (VPDB) and -6 to +2‰ under C_4 plants (Clark and Fritz, 1997; McDermott, 2004). Assuming open system conditions, Mukalla Cave speleothem $\delta^{13}C_{ca}$ values fall into the range of C_4 plant dominated vegetation with occasional C_3 plants (Fig. 7), indicating herbaceous semi-desert grassland environment above the cave during SAHPs 1-8.

Our data also shows that C_4 environments were present during the warm substages of MIS 5. This is in good coherence with phytolith data from the Jabal Faya archaeological site, UAE, showing denser and more diverse vegetation was present during MIS 5 than succeeding substages (Bretzke et al., 2013). Grassland taxa (*Kobus*, *Hippopotamus*, *Pelovoris*) and *H. sapiens* were uncovered from MIS 5a palaeolake sediments in the Nafud showing that grasslands were present in northern Arabia (Groucutt et al., 2018). In particularly, *Hippopotamus* is not a long-distance migratory species, and requires year-round access to water. Similarly, the MIS 5e speleothem $\delta^{13}C_{ca}$ values from Ashalim Cave, Negev, range from -8‰ to -2‰ (Vaks et al., 2010), suggesting comparable environments existed in the northern and southern extent of the Saharo-Arabian desert. Archaeological and fossils finds have demonstrated that *H. sapiens* were present in Arabia during MIS 5 interstadials (Groucutt et al., 2018). Furthermore, Mukalla Cave $\delta^{13}C_{ca}$ values are coherent with palaeontological evidences from older pluvial periods. Faunal assemblages from the Ti's al Ghadah palaeolake (MIS 9-13) exhibit large mammals from African and European sources (Thomas et al., 1998; Rosenberg et al., 2013; Stimpson et al., 2016), showing these wet periods were sufficient to sustain fauna that required a perennial water supply. Overall, our data adds to the growing evidence that the formation of widespread 'green' environments formed across Arabia during peak interglacial periods, which facilitated *H. sapiens* occupation and movement across the now desert areas of Arabia.

439 *4.1.6 Seasonality of precipitation during SAHPs*

440 Some stalagmites from Hoti Cave exhibit distinct annual layers, with a thickness varying between 0.1
441 and 1.2 mm (e.g., stalagmite H14; Cheng et al., 2009). Such layers are also visible un the MIS 5e section
442 of stalagmite H13, composed of a white porous laminae and dense translucent laminae. Their
443 presence suggests distinct seasonal changes in the drip rate in response to surface precipitation.
444 Nearly monthly resolved $\delta^{18}O_{ca}$ and $\delta^{13}C_{ca}$ profiles over 4 years (Fig. 8B; Tab. S8) show seasonal
445 variations of more than 1 ‰, where denser layers display more negative $\delta^{18}O_{ca}$ and $\delta^{13}C_{ca}$ values. We
446 suggest that these denser layers were formed during the monsoon seasons, at times of higher drip
447 rate, slower CO_2 degassing and lower evaporation of cave drip waters (Fleitmann et al., 2004). In.
448 contrast, the more porous white layers display more positive $\delta^{18}O_{ca}$ and $\delta^{13}C_{ca}$ due to a reduced drip
449 rate, resulting in greater CO_2 degassing and evaporation. Combined with δD_{FI} and $\delta^{18}O_{FI}$ values from
450 H13, the presence of annual layers during SAHP 1 (early to mid-Holocene; Cheng et al., 2009) and
451 SAHP 4 (MIS 5e; this study) and seasonal changes in $\delta^{18}O_{ca}$ and $\delta^{13}C_{ca}$ indicates that Southern Arabia
452 experienced a rainy (monsoon) season during boreal summer and a drier season during boreal winter.
453 This is in good agreement with climate simulations for MIS 5e, with simulations at 130, 125 and 120
454 ka BP (Gierz et al., 2017). These simulations show a strong increase in summer (JJA) precipitation at
455 130 and 125 ka BP, whereas no significant increase in winter (DJF) is observed in Southern Arabia (Fig.
456 8C). We can therefore exclude that increased precipitation was provided by enhanced Mediterranean
457 cyclone activity in winter/spring as suggested Enzel et al. (2015). Taken together, there is clear
458 evidence that climatic conditions during SAHPs were still characterized by a strong seasonality with
459 wet summers and rather dry winters.

460 4.2 Timing and Nature of SAHPs beyond 350 ka

461 *4.2.1 Chronology of stalagmite Y99 beyond 350 ka*

462 The identification of Y99 GIs beyond 350 ka BP is based (1) on thirty-one ^{230}Th and three U-Pb ages
463 (Tab. S1, S2 and S4), (2) macroscopic evidence for major discontinuities (e.g., abrupt changes in colour

of the fabric, abrupt changes in the frequency of laminae, finely defined and bright laminae and lateral displacements of the growth axis), and (3) abrupt shifts in $\delta^{18}O_{ca}$ over potential discontinuities (Fig. 2D). The latter are strong evidences for the termination of a SAHP, as they occur immediately before the cessation of stalagmite growth, when annual precipitation dropped below 300 mm yr^{-1} (Burns et al., 2001; Fleitmann et al., 2003b). Positive shifts in $\delta^{18}O_{ca}$ are also observed in stalagmites from Hoti Cave, where they mark a weakening and termination of pluvial monsoon periods within a few decades. This is particularly evident ~6.2 ka BP (Neff et al., 2001; Fleitmann et al., 2007; Fig. 6B). Using these criteria, we identified 12 further GIs (VI to XVIII) in stalagmite Y99. However, it is slightly more challenging to assign absolute ages to these GIs, as it becomes increasingly difficult to obtain accurate and precise ages ^{230}Th ages beyond 400 ka BP. While the chronology of Y99 GIs VI-XVIII is supported by thirty-one ^{230}Th and three U-Pb ages, ^{230}Th ages for GIs VI to VIII are not in perfect stratigraphic order, with several age reversals occurring between 400 and 550 ka BP. This is not related to analytical problems but rather caused by post-depositional mobilisation of U and Th, potential small-scale dissolution and re-precipitation of calcite or incorporation of ^{230}Th adsorbed to organic acids (Borsato et al., 2003; Scholz et al., 2014). These effects can imply localized open-system behaviour (Bajo et al, 2016). While post-depositional leaching of U would lead to older ages, re-precipitation of calcite or incorporation of ^{230}Th would result in younger ages as observed in some GIs. All these effects are critical for very old samples that are close to the ^{230}Th-dating limit of ~500-600 ka as even minute post-depositional alterations and several phases of dissolution and/or re-precipitation can have significant effects on the age. The higher porosity and micro-voids make in the upper section of stalagmite Y99 (Fig. 2A and B) more prone to post-depositional loss or addition of radionuclides. In contrast, the lower part of Y99, comprising GIs IX to XVIII, is composed of very dense calcite but too old for the ^{230}Th-dating method. Nevertheless, two U-Pb ages determined in different laboratories are consistent and date the base of stalagmite Y99 to 1.07 ± 0.04 Ma (GI XVIII; MIS 31). One additional U-Pb age of 0.85 ± 0.07 Ma BP for GI XII serves as an additional tie point for the chronology of the lower part of stalagmite Y99. Based on the consistent pattern of high-monsoonal rainfall and stalagmite growth

during interglacial intervals during the last 350 ka BP (Fig. 4), we used orbital tuning to the LR04 stack (Lisiecki and Raymo, 2005) to assign absolute ages for Y99 GIs VI to XIII and XIV to XVII (Fig. 9). The good match between the number of identified GIs and peak interglacial periods gives credence to the Y99 chronology.

4.2.2 Climate and environmental conditions in Southern Arabia over the last 1.1 Ma

At least 21 SAHPs occurred over the last 1.1 Ma at times when low ice volume and high summer insolation strengthened both the ISM and ASM. AS mentioned previously, there is a general scarcity of terrestrial records covering more than 400 to 500 ka BP in Northern Africa and the Arabian Peninsula, and marine sediments are the only source of information. Two dust records from the Eastern Mediterranean (ODP 967; Grant et al., 2017) and Arabian Sea (ODP 721/722; deMenocal et al., 1995) extend beyond 500 ka BP and are interpreted to reflect continental wetness in the wider northeast African region and the Arabian Peninsula (Fig. 10). The ODP 967 PCA index of rainfall and aridity (PC2; Fig. 10) is based on trace element content (e.g., titanium) and sapropels and shows distinct fluctuations in the strength and spatial extent of the ASM. The ODP 967 record thus provides evidence for multiple “Green Sahara Periods”. When compared to the stalagmite record of SAHPs, some wet periods in the ODP 967 record coincide with SAHPs, such as during the early to middle Holocene, MIS 5e, 7a, 9e and 13a (Fig. 10). There are also notable differences and wet climatic phases in the ODP 967 PC2 record are not always consistent with SAHPs, such as MIS 6 or MIS 16. Adversely, between 950-650 ka BP, the ODP 967 rainfall index is typically in a ‘dry’ mode while at least three SAHPs occurred within MIS 17, 19 and 21. Likewise, the association between SAHPs and low dust content in the ODP 721/722 core is not always evident. For instance, dust content is relatively low and constant between MISs 12 and 16, suggesting rather humid climatic conditions between 425 and 675 ka BP. The discrepancy between dust and stalagmite records has been observed before (Fleitmann et al., 2011) and could be related to regional variability, availability of dust and changes in wind direction and strength.

Stalagmite Y99 $\delta^{18}O_{ca}$ values of all GIs are very similar and typically range from -7 to -11 ‰ (Fig. 9), indicating that the ASM was the dominant source of precipitation during all SAHPs. There are, however, differences in the degree of wetness between SAHPs as more negative $\delta^{18}O_{ca}$ values indicate higher ASM and ISM rainfall in Yemen and Oman. The boxplot (Fig. 9) of $\delta^{18}O_{ca}$ values of all Mukalla Cave stalagmites show that SAHPs 4, 5, 18, 19 and 20 exhibit the most negative $\delta^{18}O_{ca}$ values and are thus characterized by the highest monsoonal rainfall.

Y99 $\delta^{13}C_{ca}$ values range 2 to -8‰ (Fig. 9) and differences are apparent between SAHPs. As stated above, these ranges are typical of C_4 environments above the cave assuming 'open system' conditions. However, $\delta^{13}C_{ca}$ values can be influenced by various parameters such as vegetation type and density, soil thickness and moisture, as well as atmospheric and other processes (McDermott, 2004; Rowe et al., 2012). Moreover, deluge of thin soils at times of very high rainfall can lead to more positive speleothem $\delta^{13}C_{ca}$ values due to rapid infiltration into the karst system and reduced interaction with soil CO_2 (e.g., Bar-Matthews et al., 2003). Increased rainfall during SAHP 19-20 could have led to more positive $\delta^{13}C_{ca}$ values. In contrast, reduced rainfall and increased interaction of percolating water with soil CO_2 may have had the opposite effect, contributing to more negative $\delta^{13}C_{ca}$ values during SAHP 14-17. Due to the numerous controls on speleothem $\delta^{13}C_{ca}$, alterations of the principal determinant can be expected over such a long period of time. Despite this, the overall range of $\delta^{13}C_{ca}$ values indicates C_4 grasslands were present during SAHP VI-XVII. This shows that interglacial periods routinely saw vegetation form in the now desert areas of southwestern Arabia.

4.3 Hominin migrations

4.3.1 Early-Middle Pleistocene

Estimates for the potential timing of hominin dispersals during the last few hundred thousand years are mostly modelled on palaeoclimate conditions of East Africa (deMenocal, 1995; Shultz and Maslin, 2013; Maslin et al., 2014) or Eurasia (Muttoni et al., 2010; Kahlke et al., 2011). These models do not consider whether and when the Saharo-Arabian desert was traversable. Yet the formation of so called

"green corridors" between sub-Saharan Africa, northern Africa and Eurasia created "windows of opportunity" that would have been critical for hominin occupation and dispersal. Though, it is surely more apt to consider these areas as "green landscapes" in which hominin populations inhabited – rather than a route to the 'other' side. Based on the timing of SAHPs and their close connection to humid intervals in Northern Africa, we suggest that the Saharo-Arabian grasslands could facilitate occupation and dispersal during MIS 31 (~1080 ka: SAHP 21), MIS 29 (~1014 ka: SAHP 20), MIS 28b (~1000 ka: SAHP 19) MIS 27a (~982 ka: SAHP 18) MIS 25 (~955 ka: SAHP 17), MIS 21 (~850 ka: SAHP 16) and MIS 19 (~760 ka: SAHP 15) (Fig. 10). Frequent windows of opportunity take place between SAHP 21 to SAHP 17 (MIS 31 to MIS 25), varying between 40-10 ka intervals. SAHP 21 to 18 are also marked as some of the most negative $\delta^{18}O_{ca}$ values in Y99 (Fig. 8), indicating intense monsoon periods. Succeeding this, SAHPs reduced in frequency, with ~100-70 ka intervals between SAHPs 17-13 (MIS 25-15e). These are also marked by increased $\delta^{18}O_{ca}$ values – indicating somewhat drier periods – and reduced occurrence of Mediterranean sapropels (Fig. 10). This shift echoes the transition from ~40 ka to ~100 ka glacial interglacial cycles, known as the Middle Pleistocene Transition (MPT) (Lisiecki and Raymo, 2005; Railsback et al., 2015; Tzedakis et al., 2017). Thus, it is likely that the pattern of hominin occupation of Arabia shift in line with this transition, with longer gaps between occupations phases. However, we must emphasise that direct ages have not been attained for SAHPs 20-17 and 19-13, meaning this argument is currently somewhat tentative. Attaining direct ages for these SAHPs should be a target of future analysis.

The early appearance of *H. heidelbergensis* at Melka Kunture (Ethiopia) soon after ~875 ± 10 ka (MIS 21; Profico et al., 2016) and subsequent appearances in Eurasia is a key event in Early-Middle Pleistocene hominin evolution. SAHPs within this period provide potential timings for *H. heidelbergensis* dispersal, assuming an African origin for this species. While there is a paucity of absolute dating, Oldowan and Acheulean tool typologies have been uncovered in Southern Arabia (Chauhan, 2009; Groucutt and Petraglia, 2012 and references therein; Bailey et al., 2015; Bretzke et al., 2016). This suggests an additional behavioural adaptation was not required for Mode-1 or Mode-

2 bearing hominins to occupy Arabia, at least as represented by the lithic record, but occupation was likely dependent on periods of ameliorated climatic conditions. Here, we have provided timings in which the Arabian Peninsula was occupiable and traversable.

SAHPs during MIS 17 (~700 ka: SAHP 14), MIS 15e (~600 ka: SAHP 13), MIS 15a (~675 ka: SAHP 12), MIS 13c (~530 ka: SAHP 11) and MIS 13a (~480 ka: SAHP 10) may have facilitated dispersals from Africa. Y99 $\delta^{18}O_{ca}$ have positive (SAHP 14 and 13) and variable (SAHP 12, 11 and 10) values, indicating somewhat drier or more variable climates, respectively. Nevertheless, these values are more negative than Holocene values, demonstrating the climate was significantly wetter. As stated above, Oldowan and Acheulean sites are distributed across western and Southern Arabia (Groucutt and Petraglia, 2012), most likely representing Lower Palaeolithic occupation. In particular, flint scatters from the Nafud – found in conjunction with grassland fauna – indicates hominin occupation of Arabia during MIS 13 or 9 (Rosenberg et al., 2013; Stimpson et al., 2016; Roberts et al., 2018). While these SAHPs facilitated occupation of Arabia, it is difficult to relate these to demographic changes in Eurasia due to the persistent presence of Acheulean typologies since ~1.4 Ma (Moncel et al., 2015; Gallotti, 2016). Nonetheless, future studies of Middle Pleistocene population dynamics in Eurasia may benefit from consideration of SAHP timings.

4.3.2 Early H. sapiens *dispersal*

H. sapiens emerged as a distinct species in Africa during the Middle Pleistocene (Hublin et al., 2017; Richter et al., 2017; Scerri et al., 2018b). Behavioural and anatomical modernity evolved gradually throughout the later Middle Pleistocene and into the Upper Pleistocene (Mcbrearty and Brooks, 2000). Whilst *H. sapiens* dispersals during the Upper Pleistocene led to colonisation of Eurasia, it has been suggested that *H. sapiens* may also have dispersed within the Middle Pleistocene (Breeze et al., 2016). This may be validated by a *H. sapiens* maxilla from Misliya Cave, Israel, dated between 194 and 177 ka (Hershkovitz et al., 2018; but see Sharp and Paces, 2018). Hershkovitz et al. (2018) suggested a dispersal may have occurred during MIS 6e (~191-170 ka). Similarly, the recent identification of *H.*

591 *sapiens* at Apidima, Greece, ~210 ka (MIS 7) provides further support for earlier dispersals (Harvati et
592 al., 2019; but see Wade, 2019).

593 Travertine deposition in the Negev (Waldmann et al., 2010), increase rainfall in the Levant and Dead
594 Sea catchment (Frumkin et al., 1999; Bar-Matthews et al., 2003; Gasse et al., 2015; Torfstein et al.,
595 2015), decreased RC09-166 $\delta D_{leafwax}$ (Tierney et al., 2017), and increased Saharan run-off (Williams et
596 al., 2015) indicate ameliorated conditions which may have facilitated *H. sapiens* dispersal within MIS
597 6e (~191-170 ka) (Breeze et al., 2016; Garcea, 2016). Lack of speleothem growth at Mukalla and Hoti
598 Cave and absence of lake formations (Rosenberg et al., 2011, 2012, 2013) indicate the tropical rain
599 belt did not migrate past 14°N during MIS 6. Moreover, absence of speleothem growth in the central
600 Negev (Vaks et al., 2010) also demonstrates that winter Mediterranean precipitation regimes were
601 not substantially enhanced during MIS 6e. Without these widespread changes in regional
602 precipitation, it is unlikely that green landscapes and inter-regional range expansion could have been
603 sustained.

604 We therefore suggest dispersals may have occurred during SAHP 5 and 6 (MIS 7a and 7e). Y99 $\delta^{18}O_{ca}$
605 reveals SAHP 5 (MIS 7a) was as wet as SAHP 4 (MIS 5e: discussed below), and $\delta^{13}C_{ca}$ demonstrate a C_4
606 biome flourished (Fig. 7). Moreover, SAHP 5 (~205-195 ka) corresponds to lake formations in northern
607 Arabia (Rosenberg et al., 2013), and the Sahara (Armitage et al., 2007, 2015), central ages of palaeosol
608 formation on the Sinai Peninsula (Roskin et al., 2013) and speleothem growth in the central Negev
609 (Vaks et al., 2010). Thus, not only did pluvial landscapes connect northern Arabia and the Levant
610 (Breeze et al., 2016), but corridors connected northern and Southern Arabia. While archaeological
611 evidence for such an early dispersal is currently very limited, recent dating of the Saffaqah
612 archaeological site demonstrates hominins occupied Arabia during MIS 7, with techno-cultural
613 similarities to Mieso (Ethiopia) archaeological assemblages (Scerri et al., 2018a). Further evidence is
614 required, however, taken with recent findings from the Levant (Hershkovitz et al., 2018) and south-

615 eastern Europe (Harvati et at., 2019), our data suggests MIS 7a enhancement of the monsoon domain
616 could have facilitated *H. sapiens* range expansion into Eurasia.

617 Furthermore, our data shows that Southern Arabia could have facilitated occupation by *H. sapiens*
618 shortly after their African emergence during MIS 9 (Hublin et al., 2017; Richter et al., 2017).
619 Considering recent discussions of the pan-African origin of *H. sapiens* (Scerri et al., 2018b), we suggest
620 that Arabia may have been frequently occupied by various *H. sapiens* lineages. The role of Green
621 Arabia as a habitat for early *H. sapiens* may therefore add to ongoing discussions concerning localized
622 adaptations and genetic flow between subdivided populations (Scerri et al., 2018b). The identification
623 of favourable conditions in MIS 7 and 9 will remain of interest if *H. sapiens* are not identified: i.e. what
624 prevented their expansion into the region at these times?

625 *4.3.3 Late Pleistocene H. sapiens dispersal*

626 The dispersal of *H. sapiens* during the Late Pleistocene is a topic of intense debate, with models
627 changing frequently with new fossil finds. Generally, there is an acceptance that formation of green
628 landscapes in the Saharo-Arabian desert belt facilitated dispersals during MIS 5e (~128-121 ka), MIS
629 5c (~104-93 ka) and MIS 5a (85-71 ka) (Bae et al., 2017; Groucutt et al., 2018; Rabett, 2018), which is
630 supported by the Mukalla and Hoti Cave records. During the last 130 ka, SAHP 4 (127.8 ± 0.626 to
631 120.3 ± 0.399 ka) was the most intense pluvial period (Fig. 5), which is in good agreement with lake
632 records in Arabia (Rosenberg et al., 2011, 2012, 2013; Matter et al., 2015). Furthermore, $\delta^{13}C_{ca}$ values
633 demonstrate a grassland environment flourished in the now desert areas of Yemen (Fig 6), which is
634 corroborated by phytolith evidence from Jabal Faya, UAE (Bretzke et al., 2013). SAHP 3 (MIS 5c) and
635 SAHP 2 (MIS 5a) are consistent with intervals of lake formations in Arabia (Petraglia et al., 2012;
636 Rosenberg et al., 2011, 2012, 2013; Parton et al., 2018) during MIS 5c and 5a and It is clear that *H.*
637 *sapiens* occupied the now desert interior of Arabia within MIS 5a (e.g., Groucutt et al., 2018).

638 A subsequent dispersal is argued to have taken place during MIS 4-3 (Mellars, 2006, 2013; Shea, 2008;
639 Rohling et al., 2013; Langgut et al., 2018). A growing body of archaeological evidence shows *H. sapiens*

640 were present in Arabia during MIS 3 (Armitage et al., 2011; Delagnes et al., 2012; Jennings et al., 2016),
641 though occupation may have been limited to punctuated pluvial periods (Groucutt and Petraglia,
642 2012). Whether these could have facilitated more widespread dispersals is a subject of controversial
643 debate (Mellars et al., 2006; Groucutt et al., 2015a; Bae et al., 2017). The palaeoclimatic evidence for
644 increased rainfall during MIS 4/3 is variable between records. It has been argued that punctuated
645 humid intervals in northern Africa and Levant may have facilitated dispersal during MIS 4-3 (Hoffmann
646 et al., 2016; Langgut et al., 2018). However, the lack of speleothem growth in southern Arabia during
647 MIS 4-3 suggest that the ASM was considerably weaker and did not penetrate into the Arabian
648 Peninsula. Our assumption is supported by more positive $\delta D_{leafwax}$ values in Core RC09-166 from the
649 Gulf of Aden (Fig. 4), indicating lower monsoonal rainfall compared to MIS 5a or the early to middle
650 Holocene in the Horn of Africa and Afar regions. Additional supporting evidence comes from median
651 grain sizes in cores KL 11 (Red Sea) and KL 15 (Gulf of Aden) which are also larger and indicative of
652 more arid climatic conditions during MIS 4-3 (Fig. 4). In contrast, palaeolake formation in the Nafud
653 (northern Saudi Arabia) (Parton et al., 2018) and fluvial activity at Al-Quwaiayh, central Saudi Arabia
654 (McLaren et al., 2009) Yemen (Delagnes et al., 2012), and in Oman (Blechschmidt et al., 2009; Parton
655 et al., 2013, 2015; Hoffmann et al., 2015) have been dated to early MIS 3. Records in Southern Arabia
656 are not corroborated by speleothem growth at Mukalla Cave or Hoti Cave, indicating that the tropical
657 rain-belt was suppressed. This discrepancy may stem from the potential for fluvio-lacustrine and
658 alluvial records to record high intensity, but brief, storm and flooding events (e.g., Rosenberg et al.,
659 2012; Hoffmann et al., 2015); whereas speleothems require prolonged and more substantial changes
660 in regional rainfall. Moreover, brief and intense storms currently occur under modern climates during
661 hot summers, which could mean MIS 3 alluvial records show precipitation regimes were not greatly
662 different than current conditions (Hoffmann et al., 2015). Taken together, MIS 3 precipitation may not
663 have been sustained or intense enough to have substantially impacted environments in Southern
664 Arabia. Despite archaeological evidence for MIS 3 occupation, our findings suggest that MIS 5
665 interstadials were 'climatic optima' for hominin dispersal; whereas *H. sapiens* dispersal opportunities

during MIS 3 may have been more limited or required different behavioral adaptations. If, however, MIS 3 environments could not sustain dispersal (meaning MIS 3 populations can be related to groups that entered during MIS 5), this implies *H. sapiens* persistence during MIS 4, a time with very limited evidence for ameliorated conditions (Parton et al., 2015).

5. Conclusion

New ^{230}Th and U-Pb dates for stalagmite Y99 from Mukalla Cave in Yemen allow to extend the speleothem-based record of continental wetness back to 1.1 Ma BP. In combination with previously published stalagmite records from Southern Arabia (Burns et al., 2001; Fleitmann et al., 2011), at least twenty-one humid intervals with precipitation above ~300 mm yr^{-1} developed in Southern Arabia, all them occurred during peak interglacial periods. Of all SAHPs the early to mid-Holocene humid period was the least humid period. Hydrogen and oxygen isotope measurements on water extracted from stalagmite fluid inclusions indicate that enhanced rainfall during SAHPs resulted from an intensification and greater range of the ASM and ISM. This assumption is further supported by the presence of annual laminae in some stalagmites and nearly monthly-resolved oxygen and carbon isotope measurements which indicate a strong seasonal climate during SAHP, with one rainy (monsoon) season during SAHPs. While there is restricted archaeological evidence for hominin occupation beyond 350 ka BP, these landscapes *could* have facilitated occupation of late *H. erectus* populations. Subsequent SAHPs may have also facilitated the dispersals of early *H. sapiens* soon after their emergence ~300 ka BP.

Acknowledgements

This work was supported by the AHRC South, West and Wales Doctoral Training Partnership (Grant AH/L503939/1) the Swiss National Science Foundation (Grant PP002-110554/1 to DF and Grant CRSI22-132646/1 to DF and ML), U.S. National Science Foundation (Grant 1702816 to RLE and HC) and the National Natural Science Foundation of China (Grant NSFC 41888101). DF acknowledges support

691 from NERC Isotope Geosciences Facilities Steering Committee (Grant IP-1376-051). We would like to
692 thank the editor and three anonymous reviewers for their constructive comments and suggestions.

693 **Appendix A. Supplementary data**

694 The following are the supplementary data to this article:

695 Fig. S1:

696 Fig. S2:

697 Fig. S3:

698 Tab. S1-S3:

699 Tab. S4-S5:

700 Tab. S5:

701 Tab. S6:

702 Tab. S7:

703 Tab. S8:

704 Tab. S9:

705 Tab. S10:

706 Tab. S11:

707 **References**

708 Affolter, S., Fleitmann, D., Leuenberger, M., 2014. New online method for water isotope analysis of
709 speleothem fluid inclusions using laser absorption spectroscopy (WS-CRDS). Climate of the
710 Past. 10, 1291–1304.

711 Affolter, S., Häuselmann, A.D., Fleitmann, D., Häuselmann, P., Leuenberger, M., 2015. Triple isotope
712 (δD, δ17O, δ18O) study on precipitation, drip water and speleothem fluid inclusions for a
713 Western Central European cave (NW Switzerland). Quaternary Science Reviews. 127, 73–89.

714 Al-ameri, A., Schneider, M., Abu Lohom, N., Sprenger, C., 2014. The Hydrogen (δD) and Oxygen
715 (δ18O) Isotopic Composition of Yemen's Rainwater. Arabian Journal for Science and
716 Engineering. 39, 423–436.

717 Almogi-Labin, A., Schmiedl, G., Hemleben, C., Siman-Tov, R., Segl, M., Meischner, D., 2000. The
718 influence of the NE winter monsoon on productivity changes in the Gulf of Aden, NW Arabian
719 Sea, during the last 530 ka as recorded by foraminifera. Marine Micropaleontology. 40, 295–
720 319.

721 Armitage, S.J., Bristow, C.S., Drake, N.A., 2015. West African monsoon dynamics inferred from
722 abrupt fluctuations of Lake Mega-Chad. Proceedings of the National Academy of Sciences. 112,
723 8543–8548.

724 Armitage, S.J., Drake, N.A., Stokes, S., El-Hawat, A., Salem, M.J., White, K., Turner, P., McLaren, S.J.,
725 2007. Multiple phases of North African humidity recorded in lacustrine sediments from the
726 Fazzan Basin, Libyan Sahara. Quaternary Geochronology. 2, 181–186.

727 Bae, C.J., Douka, K., Petraglia, M.D., 2017. On the origin of modern humans: Asian perspectives.
728 Science.

729 Bailey, G.N., Devès, M.H., Inglis, R.H., Meredith-Williams, M.G., Momber, G., Sakellariou, D., Sinclair,
730 A.G.M., Rousakis, G., Al Ghamdi, S., Alsharekh, A.M., 2015. Blue Arabia: Palaeolithic and
731 underwater survey in SW Saudi Arabia and the role of coasts in Pleistocene dispersals.
732 Quaternary International. 382, 42–57.

733 Bajo, P., Hellstrom, J., Frisia, S., Drysdale, R., Black, J., Woodhead, J., Borsato, A., Zanchetta, G.,

734 Wallce, M.W., Regattieri, E., Haese, R., 2016. Cryptic diagenesis and its implications for
735 speleothem geochronologies. 148, 17-28.

736 Baker, A., Ito, E., Smart, P.L., McEwan, R.F., 1997. Elevated and variable values of 13C in speleothems
737 in a British cave system. Chemical Geology. 136, 263–270.

738 Bar-Matthews, M., Ayalon, A., Gilmour, M., Matthews, A., Hawkesworth, C.J., 2003. Sea - land
739 oxygen isotopic relationships from planktonic foraminifera and speleothems in the Eastern
740 Mediterranean region and their implication for paleorainfall during interglacial intervals.
741 Geochimica et Cosmochimica Acta. 67, 3181–3199.

742 Bar-Matthews, M., Ayalon, A., Matthews, A., Sass, E., Halicz, L., 1996. Carbon and oxygen isotope
743 study of the active water-carbonate system in a karstic Mediterranean cave: Implications for
744 paleoclimate research in semiarid regions. Geochimica et Cosmochimica Acta. 60, 337–347.

745 Beck, J.W., Zhou, W., Li, C., Wu, Z., White, L., Xian, F., Kong, X., An, Z., 2018. A 550,000-year record of
746 East Asian monsoon rainfall from 10Be in loess. Science. 360, 877 LP – 881.

747 Berger, A., Loutre, M.F., 1991. Insolation values for the climate of the last 10 million years.
748 Quaternary Science Reviews. 10, 297–317.

749 Berger, A., Loutre, M.F., 1999. Parameters of the Earths orbit for the last 5 Million years in 1 kyr
750 resolution. Supplement to: Berger, A; Loutre, M F (1991): Insolation values for the climate of
751 the last 10 million of years. Quaternary Science Reviews, 10(4), 297-317, doi:10.1016/0277-
752 3791(91)90033-Q.

753 Blechschmidt, I., Matter, A., Preusser, F., Rieke-Zapp, D., 2009. Monsoon triggered formation of
754 Quaternary alluvial megafans in the interior of Oman. Geomorphology.

755 Borsato, A., Quinif, Y., Bini, A., Dublyansky, Y., 2003. Open-system alpine speleothems: implications
756 for U-series dating and palaeoclimate reconstructions. Studi Trentini di Scienze Naturali – Acta

Geologica. 80, 71-83.

Breeze, P.S., Drake, N.A., Groucutt, H.S., Parton, A., Jennings, R.G.P., White, T.S., Clark-Balzan, L., Shipton, C., Scerri, E.M.L.L., Stimpson, C.M., Crassard, R., Hilbert, Y., Alsharekh, A., Al-Omari, A., Petraglia, M.D., Clarke-Balzan, L., Shipton, C., White, T.S., Scerri, E.M.L.L., Stimpson, C.M., Clark-Balzan, L., Shipton, C., Scerri, E.M.L.L., Stimpson, C.M., Crassard, R., Hilbert, Y., Alsharekh, A., Al-Omari, A., Petraglia, M.D., 2015. Remote sensing and GIS techniques for reconstructing Arabian palaeohydrology and identifying archaeological sites. Quaternary International. 382, 98–119.

Breeze, P.S., Groucutt, H.S., Drake, N.A., White, T.S., Jennings, R.P., Petraglia, M.D., 2016. Palaeohydrological corridors for hominin dispersals in the Middle East ~250-70,000 years ago. Quaternary Science Reviews. 144, 155–185.

Bretzke, K., Armitage, S.J., Parker, A.G., Walkington, H., Uerpmann, H.P., 2013. The environmental context of Paleolithic settlement at Jebel Faya, Emirate Sharjah, UAE. Quaternary International. 300, 83–93.

Bretzke, K., Yousif, E., Jasim, S., 2016. Filling in the gap - The Acheulean site Suhailah 1 from the central region of the Emirate of Sharjah, UAE. Quaternary International.

Burns, S.J., Fleitmann, D., Matter, A., Neff, U., Mangini, A., 2001. Speleothem evidence from Oman for continental pluvial events during interglacial periods. Geology. 29, 623–626.

Burns, S.J., Matter, A., Frank, N., Mangini, A., 1998. Speleothem-based paleoclimate record from northern Oman. Geology. 26, 499–502.

Cerling, T.E., Wynn, J.G., Andanje, S.A., Bird, M.I., Korir, D.K., Levin, N.E., MacE, W., MacHaria, A.N., Quade, J., Remien, C.H., 2011. Woody cover and hominin environments in the past 6-million years. Nature. 476, 51–56.

780 Chauhan, P.R., 2009. Early Homo Occupation Near the Gate of Tears: Examining the
781 Paleoanthropological Records of Djibouti and Yemen. In: Vertebrate Paleobiology and
782 Paleoanthropology.

783 Cheng, H., Edwards, R.L., Sinha, A., Spötl, C., Yi, L., Chen, S., Kelly, M., Kathayat, G., Wang, X., Li, X.,
784 Kong, X., Wang, Y., Ning, Y., Zhang, H., 2016. The Asian monsoon over the past 640,000 years
785 and ice age terminations. Nature. 534, 640–646.

786 Cheng, H., Fleitmann, D., Edwards, R.L., Wang, X., Cruz, F.W., Auler, A.S., Mangini, A., Wang, Y., Kong,
787 X., Burns, S.J., Matter, A., 2009. Timing and structure of the 8.2. kyr B.P. event inferred from δ
788 18O records of stalagmites from China, Oman, and Brazil. Geology. 37, 1007–1010.

789 Cheng, H., Lawrence Edwards, R., Shen, C.C., Polyak, V.J., Asmerom, Y., Woodhead, J., Hellstrom, J.,
790 Wang, Y., Kong, X., Spötl, C., Wang, X., Calvin Alexander, E., 2013. Improvements in ^{230}Th
791 dating, ^{230}Th and ^{234}U half-life values, and U-Th isotopic measurements by multi-collector
792 inductively coupled plasma mass spectrometry. Earth and Planetary Science Letters. 371–372,
793 82–91.

794 Clark, I., Fritz, P., 1997. Environmnetal Istopes in Hydrogeology. Lewis Publishers, New York.

795 Clemens, S.C., Prell, W.L., 2003. A 350,000 year summer-monsoon multi-proxy stack from the Owen
796 Ridge, Northern Arabian Sea. In: Marine Geology. pp. 35–51.

797 Coogan, L.A., Parrish, R.R., Roberts, N.M.W., 2016. Early hydrothermal carbon uptake by the upper
798 oceanic crust: Insight from in situ U-Pb dating. Geology.

799 Crémière, A., Lepland, A., Chand, S., Sahy, D., Condon, D.J., Noble, S.R., Martma, T., Thorsnes, T.,
800 Sauer, S., Brunstad, H., 2016. Timescales of methane seepage on the Norwegian margin
801 following collapse of the Scandinavian Ice Sheet. Nature Communications.

802 Dansgaard, W., 1964. Stable isotopes in precipitation. Tellus. 16, 436–468.

803 Delagnes, A., Tribolo, C., Bertran, P., Brenet, M., Crassard, R., Jaubert, J., Khalidi, L., Mercier, N.,
804 Nomade, S., Peigné, S., Sitzia, L., Tournepiche, J-F., Al-Halibi, M., Al-Mosabi, A., Macchiarelli, R.,
805 2012. Inland human settlement in southern Arabia 55,000 years ago. New evidence from the
806 Wadi Surdud Middle Palaeolithic site complex, western Yemen. Journal of Human Evolution.
807 63, 452–474.

808 deMenocal, P.B., 1995. Plio-Pleistocene African Climate. Science. 270, 53–59.

809 Dennis, P.F., Rowe, P.J., Atkinson, T.C., 2001. The recovery and isotopic measurement of water from
810 fluid inclusions in speleothems. Geochimica et Cosmochimica Acta. 65, 871–884.

811 Drake, N., Breeze, P., 2016. Climate Change and Modern Human Occupation of the Sahara from MIS
812 6-2. In: Africa from MIS 6-2. pp. 103–122.

813 Drake, N.A., Blench, R.M., Armitage, S.J., Bristow, C.S., White, K.H., 2011. Ancient watercourses and
814 biogeography of the Sahara explain the peopling of the desert. Proceedings of the National
815 Academy of Sciences. 108, 458–462.

816 El-Shenawy, M.I., Kim, S.-T., Schwarcz, H.P., Asmerom, Y., Polyak, V.J., 2018. Speleothem evidence
817 for the greening of the Sahara and its implications for the early human dispersal out of sub-
818 Saharan Africa. Quaternary Science Reviews. 188, 67–76.

819 Engel, M., Matter, A., Parker, A.G., Parton, A., Petraglia, M.D., Preston, G.W., Preusser, F., 2017.
820 Lakes or wetlands? A comment on 'The middle Holocene climatic records from Arabia:
821 Reassessing lacustrine environments, shift of ITCZ in Arabian Sea, and impacts of the southwest
822 Indian and African monsoons' by Enzel et al. Global and Planetary Change.

823 Enzel, Y., Kushnir, Y., Quade, J., 2015. The middle Holocene climatic records from Arabia: Reassessing
824 lacustrine environments, shift of ITCZ in Arabian Sea, and impacts of the southwest Indian and
825 African monsoons. Global and Planetary Change.

826 Fernandes, C.A., Rohling, E.J., Siddall, M., 2006. Absence of post-Miocene Red Sea land bridges:
827 Biogeographic implications. Journal of Biogeography.

828 Fleitmann, D., 1997. Klastischer Eintrag in das Rote Meer und den Golf von Aden durch den
829 Arabischen Monsun-Untersuchungen an Kolbenlot-Kernen. Diplom-Arbeit, Institut und
830 Museum für Geologie und Paläontologie der Georg-August-Universität zu Göttingen.

831 Fleitmann, D., Burns, S.J., Mangini, A., Mudelsee, M., Kramers, J., Villa, I., Neff, U., Al-Subbary, A.A.,
832 Buettner, A., Hippler, D., Matter, A., 2007. Holocene ITCZ and Indian monsoon dynamics
833 recorded in stalagmites from Oman and Yemen (Socotra). Quaternary Science Reviews. 26,
834 170–188.

835 Fleitmann, D., Burns, S.J., Mudelsee, M., Neff, U., Kramers, J., Mangini, A., Matter, A., 2003a.
836 Holocene forcing of the Indian monsoon recorded in a stalagmite from Southern Oman.
837 Science. 300, 1737–1739.

838 Fleitmann, D., Burns, S.J., Neff, U., Mangini, A., Matter, A., 2003b. Changing moisture sources over
839 the last 330,000 years in Northern Oman from fluid-inclusion evidence in speleothems.
840 Quaternary Research. 60, 223–232.

841 Fleitmann, D., Burns, S.J., Neff, U., Mudelsee, M., Mangini, A., Matter, A., 2004. Palaeoclimatic
842 interpretation of high-resolution oxygen isotope profiles derived from annually laminated
843 speleothems from Southern Oman. In: Quaternary Science Reviews. pp. 935–945.

844 Fleitmann, D., Burns, S.J., Pekala, M., Mangini, A., Al-Subbary, A., Al-Aowah, M., Kramers, J., Matter,
845 A., 2011. Holocene and Pleistocene pluvial periods in Yemen, southern Arabia. Quaternary
846 Science Reviews. 30, 783–787.

847 Fleitmann, D., Matter, A., 2009. The speleothem record of climate variability in Southern Arabia.
848 Comptes Rendus - Geoscience. 341, 633–642.

849 Fick, S.E., Hijmans, R.J., 2017. Worldclim 2: New 1-km spatial resolution climate surfaces for global
850 land areas. International Journal of Climatology. 37, 4302–4315.

851 Frumkin, A., Ford, D.C., Schwarcz, H.P., 1999. Continental oxygen isotopic record of the last 170,000
852 years in Jerusalem. Quaternary Research. 51, 317–327.

853 Gallotti, R., 2016. The East African origin of the Western European Acheulean technology: Fact or
854 paradigm? Quaternary International. 411, 9–24.

855 Garcea, E.A.A., 2016. Dispersals Out of Africa and Back to Africa: Modern origins in North Africa.
856 Quaternary International. 408, 79–89.

857 Gasse, F., Vidal, L., Van Campo, E., Demory, F., Develle, A.L., Tachikawa, K., Elias, A., Bard, E., Garcia,
858 M., Sonzogni, C., Thouveny, N., 2015. Hydroclimatic changes in northern Levant over the past
859 400,000 years. Quaternary Science Reviews.

860 Gat, J.R., Carmi, I., 1970. Evolution of the isotopic composition of atmospheric waters in the
861 Mediterranean Sea area. Journal of Geophyscial Research. 75, 3039–3048.

862 Gierz, P., Werner, M., Lohmann, G., 2017. Simulating climate and stable water isotopes during the
863 Last Interglacial using a coupled climate-isotope model. Journal of Advances in Modeling Earth
864 Systems. 9, 2027–2045.

865 Grant, K.M., Grimm, R., Mikolajewicz, U., Marino, G., Ziegler, M., Rohling, E.J., 2016. The timing of
866 Mediterranean sapropel deposition relative to insolation, sea-level and African monsoon
867 changes. Quaternary Science Reviews. 140, 125–141.

868 Grant, K.M., Rohling, E.J., Bar-Matthews, M., Ayalon, A., Medina-Elizalde, M., Ramsey, C.B., Satow,
869 C., Roberts, A.P., 2012. Rapid coupling between ice volume and polar temperature over the
870 past 50,000 years. Nature. 491, 744–747.

871 Grant, K.M., Rohling, E.J., Westerhold, T., Zabel, M., Heslop, D., Konijnendijk, T., Lourens, L., 2017. A

3 million year index for North African humidity/aridity and the implication of potential pan-African Humid periods. Quaternary Science Reviews. 171, 100–118.

Groucutt, H.S., Grün, R., Zalmout, I.A.S., Drake, N.A., Armitage, S.J., Candy, I., Clark-Wilson, R., Louys, J., Breeze, P.S., Duval, M., Buck, L.T., Kivell, T.L., Pomeroy, E., Stephens, N.B., Stock, J.T., Stewart, M., Price, G.J., Kinsley, L., Sung, W.W., Alsharekh, A., Al-Omari, A., Zahir, M., Memesh, A.M., Abdulshakoor, A.J., Al-Masari, A.M., Bahameem, A.A., Al Murayyi, K.M.S., Zahrani, B., Scerri, E.L.M., Petraglia, M.D., Gramp, R., S Zalmout, I.A., Drake, N.A., Armitage, S.J., Candy, I., Clark-Wilson, R., Louys, J., Breeze, P.S., Duval, M., Buck, L.T., Kivell, T.L., Pomeroy, E., Stephens, N.B., Stock, J.T., Stewart, M., Price, G.J., Kinsley, L., Wai Sung, W., Alsharekh, A., Al-Omari, A., Zahir, M., Memesh, A.M., Abdulshakoor, A.J., Al-Masari, A.M., Bahameem, A.A., S Al Murayyi, K.M., Zahrani, B., M Scerri, E.L., Petraglia, M.D., 2018. Homo sapiens in Arabia by 85,000 years ago. Nature Ecology & Evolution.

Groucutt, H.S., Petraglia, M.D., 2012. The prehistory of the Arabian peninsula: Deserts, dispersals, and demography. Evolutionary Anthropology. 21, 113–125.

Groucutt, H.S., Petraglia, M.D., Bailey, G., Scerri, E.M.L.L., Parton, A., Clark-Balzan, L., Jennings, R.P., Lewis, L., Blinkhorn, J., Drake, N.A., Breeze, P.S., Inglis, R.H., Dev??s, M.H., Meredith-Williams, M., Boivin, N., Thomas, M.G., Scally, A., Devès, M.H., Meredith-Williams, M., Boivin, N., Thomas, M.G., Scally, A., 2015a. Rethinking the dispersal of Homo sapiens out of Africa. Evolutionary Anthropology. 24, 149–164.

Groucutt, H.S., Shipton, C., Alsharekh, A., Jennings, R., Scerri, E.M.L., Petraglia, M.D., 2015b. Late Pleistocene lakeshore settlement in northern Arabia: Middle Palaeolithic technology from Jebel Katefeh, Jubbah. Quaternary International. 382, 215–236.

Harvati, K., Röding, C., Bosman, A.M., Karakostis, F.A., Grün, R., Stringer, C., Karkanas, P., Thompson, N.C., Koutoulidis, V., Moulopoulos, L.A., Gorgoulis, V.G., Kouloukoussa, M., 2019. Apidima Cave

fossils provide earliest evidence of *Homo sapiens* in Eurasia. Nature. 571, 500–504.

Herold, M., Lohmann, G., 2009. Eemian tropical and subtropical African moisture transport: An isotope modelling study. Climate Dynamics. 33, 1075–1088.

Hershkovitz, I., Weber, G.W., Quam, R., Duval, M., Grün, R., Kinsley, L., Ayalon, A., Bar-Matthews, M., Valladas, H., Mercier, N., Arsuaga, J.L., Martinón-Torres, M., Bermúdez de Castro, J.M., Fornai, C., Martín-Francés, L., Sarig, R., May, H., Krenn, V.A., Slon, V., Rodríguez, L., García, R., Lorenzo, C., Carretero, J.M., Frumkin, A., Shahack-Gross, R., Bar-Yosef Mayer, D.E., Cui, Y., Wu, X., Peled, N., Groman-Yaroslavski, I., Weissbrod, L., Yeshurun, R., Tsatskin, A., Zaidner, Y., Weinstein-Evron, M., 2018. The earliest modern humans outside Africa. Science. 359, 456 LP – 459.

Hill, C.A., Polyak, V.J., Asmerom, Y., P. Provencio, P., 2016. Constraints on a Late Cretaceous uplift, denudation, and incision of the Grand Canyon region, southwestern Colorado Plateau, USA, from U-Pb dating of lacustrine limestone. Tectonics. 35, 896–906.

Hoffmann, D.L., Rogerson, M., Spötl, C., Luetscher, M., Vance, D., Osborne, A.H., Fello, N.M., Moseley, G.E., 2016. Timing and causes of North African wet phases during the last glacial period and implications for modern human migration. Scientific Reports. 6.

Hoffmann, G., Rupprechter, M., Rahn, M., Preusser, F., 2015. Fluvio-Lacustrine deposits reveal precipitation pattern in SE Arabia during early MIS 3. Quaternary International. 382, 145–153.

Hublin, J.J., Ben-Ncer, A., Bailey, S.E., Freidline, S.E., Neubauer, S., Skinner, M.M., Bergmann, I., Le Cabec, A., Benazzi, S., Harvati, K., Gunz, P., 2017. New fossils from Jebel Irhoud, Morocco and the pan-African origin of Homo sapiens. Nature. 546, 289–292.

Jennings, R.P., Shipton, C., Breeze, P., Cuthbertson, P., Bernal, M.A., Wedage, W.M.C.O., Drake, N.A., White, T.S., Groucutt, H.S., Parton, A., Clark-Balzan, L., Stimpson, C., al Omari, A.A., Alsharekh,

A., Petraglia, M.D., 2015a. Multi-scale Acheulean landscape survey in the Arabian Desert. Quaternary International. 382, 58–81.

Jennings, R.P., Singarayer, J., Stone, E.J., Krebs-Kanzow, U., Khon, V., Nisancioglu, K.H., Pfeiffer, M., Zhang, X., Parker, A., Parton, A., Groucutt, H.S., White, T.S., Drake, N.A., Petraglia, M.D., 2015b. The greening of Arabia: Multiple opportunities for human occupation of the Arabian Peninsula during the Late Pleistocene inferred from an ensemble of climate model simulations. Quaternary International. 382, 181–199.

Kahlke, R.D., García, N., Kostopoulos, D.S., Lacombat, F., Lister, A.M., Mazza, P.P.A., Spassov, N., Titov, V. V., 2011. Western Palaearctic palaeoenvironmental conditions during the Early and early Middle Pleistocene inferred from large mammal communities, and implications for hominin dispersal in Europe. Quaternary Science Reviews.

Kutzbach, J.E., Chen, G., Cheng, H., Edwards, R.L., Liu, Z., 2014. Potential role of winter rainfall in explaining increased moisture in the Mediterranean and Middle East during periods of maximum orbitally-forced insolation seasonality. Climate Dynamics. 42, 1079–1095.

Lambeck, K., Purcell, A., Flemming, N.C., Vita-Finzi, C., Alsharekh, A.M., Bailey, G.N., 2011. Sea level and shoreline reconstructions for the Red Sea: Isostatic and tectonic considerations and implications for hominin migration out of Africa. Quaternary Science Reviews.

Langgut, D., Almogi-Labin, A., Bar-Matthews, M., Pickarski, N., Weinstein-Evron, M., 2018. Evidence for a humid interval at ~56–44 ka in the Levant and its potential link to modern humans dispersal out of Africa. Journal of Human Evolution. 124, 75–90.

Larrasoaña, J.C., Roberts, A.P., Rohling, E.J., 2013. Dynamics of Green Sahara Periods and Their Role in Hominin Evolution. PLoS ONE. 8.

Larrasoana, J.C., Roberts, A.P., Rohling, E.J., Winklhofer, M., Wehausen, R., 2003. Three million years

942 of monsoon variability over the northern Sahara. Climate Dynamics. 21, 689–698.

943 Lisiecki, L.E., Raymo, M.E., 2005. A Pliocene-Pleistocene stack of 57 globally distributed benthic δ
944 18O records. Paleoceanography. 20, 1–17.

945 Maslin, M.A., Brierley, C.M., Milner, A.M., Shultz, S., Trauth, M.H., Wilson, K.E., 2014. East african
946 climate pulses and early human evolution. Quaternary Science Reviews.

947 Matthews, A., Ayalon, A., Bar-Matthews, M., 2000. D/H ratios of fluid inclusions of Soreq Cave
948 (Israel) speleothems as a guide to the Eastern Mediterranean Meteoric Line relationship in the
949 last 120 kyr. Chemical Geology. 166, 183-191.

950 Matter, A., Neubert, E., Preusser, F., Rosenberg, T., Al-Wagdani, K., 2015. Palaeo-environmental
951 implications derived from lake and sabkha deposits of the southern Rub' al-Khali, Saudi Arabia
952 and Oman. Quaternary International. 382, 120–131.

953 Mcbrearty, S., Brooks, A.S., 2000. The revolution that wasn't: A new interpretation of the origin of
954 modern human behavior. Journal of Human Evolution.

955 McDermott, F., 2004. Palaeo-climate reconstruction from stable isotope variations in speleothems: A
956 review. In: Quaternary Science Reviews. pp. 901–918.

957 McGarry, S., Bar-Matthews, M., Matthews, A., Vaks, A., Schilman, B., Ayalon, A., 2004. Con-straints
958 on hydrological and paleotemperature variations in the Eastern Mediterra-nean region in the
959 last 140 ka given by the δD values of speleothem fluid inclusions. Quaternary Science Reviews.
960 23, 919–934.

961 McLaren, S.J., Al-Juaidi, F., Bateman, M.D., Millington, A.C., 2009. First evidence for episodic flooding
962 events in the arid interior of central Saudi Arabia over the last 60 ka. Journal of Quaternary
963 Science. 24, 198–207.

964 Meckler, A.N., Affolter, S., Dublyansky, Y. V., Krüger, Y., Vogel, N., Bernasconi, S.M., Frenz, M., Kipfer,

R., Leuenberger, M., Spötl, C., Carolin, S., Cobb, K.M., Moerman, J., Adkins, J.F., Fleitmann, D., 2015. Glacial-interglacial temperature change in the tropical West Pacific: A comparison of stalagmite-based paleo-thermometers. Quaternary Science Reviews. 127, 90–116.

Mellars, P., 2006. Why did modern human populations disperse from Africa ca. 60,000 years ago? A new model. Proceedings of the National Academy of Sciences. 103, 9381–9386.

Mellars, P., Gori, K.C., Carr, M., Soares, P.A., Richards, M.B., 2013. Genetic and archaeological perspectives on the initial modern human colonization of southern Asia. Preceedings of the National Academy of Sciences. 110, 10699–10704.

Mitchell, T.D., Jones, P.D., 2005. An improved method of constructing a database of monthly climate observations and associated high-resolution grids. International Journal of Climatology. 25, 693–712.

Moncel, M.H., Ashton, N., Lamotte, A., Tuffreau, A., Cliquet, D., Despriée, J., 2015. The Early Acheulian of north-western Europe. Journal of Anthropological Archaeology. 40, 302–331.

Muttoni, G., Scardia, G., Kent, D. V., 2010. Human migration into Europe during the late Early Pleistocene climate transition. Palaeogeography, Palaeoclimatology, Palaeoecology. 296, 79–93.

Neff, U., Burns, S.J., Mangini, A., Mudelsee, M., Fleitmann, D., Matter, A., 2001. Strong coherence between solar variability and the monsoon in Oman between 9 and 6 kyr ago. Nature. 411, 290–293.

Parton, A., Clark-Balzan, L., Parker, A.G., Preston, G.W., Sung, W.W., Breeze, P.S., Leng, M.J., Groucutt, H.S., White, T.S., Alsharekh, A., Petraglia, M.D., 2018. Middle-late quaternary palaeoclimate variability from lake and wetland deposits in the Nefud Desert, Northern Arabia. Quaternary Science Reviews.

988 Parton, A., Farrant, A.R., Leng, M.J., Schwenninger, J.L., Rose, J.I., Uerpmann, H.P., Parker, A.G.,
989 2013. An early MIS 3 pluvial phase in Southeast Arabia: Climatic and archaeological
990 implications. Quaternary International.

991 Parton, A., White, T.S., Parker, A.G., Breeze, P.S., Jennings, R., Groucutt, H.S., Petraglia, M.D., 2015.
992 Orbital-scale climate variability in Arabia as a potential motor for human dispersals. Quaternary
993 International.

994 Pedgley, D.E., 1969. CYCLONES ALONG THE ARABIAN COAST. Weather. 24, 456–470.

995 Petraglia, M.D., Alsharekh, A., Breeze, P., Clarkson, C., Crassard, R., Drake, N.A., Groucutt, H.S.,
996 Jennings, R., Parker, A.G., Parton, A., Roberts, R.G., Shipton, C., Matheson, C., al-Omari, A.,
997 Veall, M.A., 2012. Hominin Dispersal into the Nefud Desert and Middle Palaeolithic Settlement
998 along the Jubbah Palaeolake, Northern Arabia. PLoS ONE. 7.

999 Petraglia, M.D., Alsharekh, A.M., Crassard, R., Drake, N.A., Groucutt, H., Parker, A.G., Roberts, R.G.,
1000 2011. Middle Paleolithic occupation on a Marine Isotope Stage 5 lakeshore in the Nefud Desert,
1001 Saudi Arabia. Quaternary Science Reviews. 30, 1555–1559.

1002 Petraglia, M.D., Parton, A., Groucutt, H.S., Alsharekh, A., 2015. Green Arabia: Human prehistory at
1003 the Crossroads of Continents. Quaternary International. 382, 1–7.

1004 Profico, A., di Vincenzo, F., Gagliardi, L., Piperno, M., Manzi, G., 2016. Filling the gap. Human cranial
1005 remains from Gombore II (Melka kunture, Ethiopia; ca. 850 ka) and the origin of Homo
1006 heidelbergensis. Journal of Anthropological Sciences. 94, 41–63.

1007 Quade, J., Dente, E., Armon, M., Ben Dor, Y., Morin, E., Adam, O., Enzel, Y., 2018. Megalakes in the
1008 Sahara? A Review. Quaternary Research (United States). 90, 253–275.

1009 Rabett, R.J., 2018. The success of failed Homo sapiens dispersals out of Africa and into Asia. Nature
1010 Ecology and Evolution.

1011 Railsback, L.B., Gibbard, P.L., Head, M.J., Voarintsoa, N.R.G., Toucanne, S., 2015. An optimized
1012 scheme of lettered marine isotope substages for the last 1.0 million years, and the
1013 climatostratigraphic nature of isotope stages and substages. Quaternary Science Reviews.

1014 Richter, D., Grün, R., Joannes-Boyau, R., Steele, T.E., Amani, F., Rué, M., Fernandes, P., Raynal, J.P.,
1015 Geraads, D., Ben-Ncer, A., Hublin, J.J., McPherron, S.P., 2017. The age of the hominin fossils
1016 from Jebel Irhoud, Morocco, and the origins of the Middle Stone Age. Nature. 546, 293–296.

1017 Roberts, N.M.W., Rasbury, E.T., Parrish, R.R., Smith, C.J., Horstwood, M.S.A., Condon, D.J., 2017. A
1018 calcite reference material for LA-ICP-MS U-Pb geochronology. Geochemistry, Geophysics,
1019 Geosystems.

1020 Roberts, P., Stewart, M., Alagaili, A.N., Breeze, P., Candy, I., Drake, N., Groucutt, H.S., Scerri, E.M.L.,
1021 Lee-Thorp, J., Louys, J., Zalmout, I.S., Al-Mufarreh, Y.S.A., Zech, J., Alsharekh, A.M., al Omari, A.,
1022 Boivin, N., Petraglia, M., 2018. Fossil herbivore stable isotopes reveal middle Pleistocene
1023 hominin palaeoenvironment in 'Green Arabia.' Nature Ecology and Evolution.

1024 Rohling, E.J., Grant, K.M., Roberts, A.P., Larrasoaña, J.-C., 2013. Paleoclimate Variability in the
1025 Mediterranean and Red Sea Regions during the Last 500,000 Years. Current Anthropology. 54,
1026 S183–S201.

1027 Rohling, E.J., Marino, G., Grant, K.M., 2015. Mediterranean climate and oceanography, and the
1028 periodic development of anoxic events (sapropels). Earth-Science Reviews.

1029 Rose, J.I., Usik, V.I., Marks, A.E., Hilbert, Y.H., Galletti, C.S., Parton, A., Geiling, J.M., Černý, V.,
1030 Morley, M.W., Roberts, R.G., 2011. The Nubian complex of Dhofar, Oman: An African Middle
1031 Stone Age industry in Southern Arabia. PLoS ONE. 6.

1032 Rosenberg, T.M., Preusser, F., Blechschmidt, I., Fleitmann, D., Jagher, R., Matter, A., 2012. Late
1033 Pleistocene palaeolake in the interior of Oman: A potential key area for the dispersal of

anatomically modern humans out-of-Africa? Journal of Quaternary Science. 27, 13–16.

Rosenberg, T.M., Preusser, F., Fleitmann, D., Schwalb, A., Penkman, K., Schmid, T.W., Al-Shanti, M.A., Kadi, K., Matter, A., 2011. Humid periods in southern Arabia: Windows of opportunity for modern human dispersal. Geology. 39, 1115–1118.

Rosenberg, T.M., Preusser, F., Risberg, J., Plikk, A., Kadi, K.A., Matter, A., Fleitmann, D., 2013. Middle and Late Pleistocene humid periods recorded in palaeolake deposits of the Nafud desert, Saudi Arabia. Quaternary Science Reviews. 70, 109–123.

Roskin, J., Katra, I., Porat, N., Zilberman, E., 2013. Evolution of Middle to Late Pleistocene sandy calcareous paleosols underlying the northwestern Negev Desert Dunefield (Israel). Palaeogeography, Palaeoclimatology, Palaeoecology. 387, 134–152.

Rowe, P.J., Mason, J.E., Andrews, J.E., Marca, A.D., Thomas, L., Van Calsteren, P., Jex, C.N., Vonhof, H.B., Al-Omari, S., 2012. Speleothem isotopic evidence of winter rainfall variability in northeast Turkey between 77 and 6 ka. Quaternary Science Reviews. 45, 60–72.

Scerri, E.M.L., Shipton, C., Clark-Balzan, L., Frouin, M., Schwenninger, J.-L., Groucutt, H.S., Breeze, P.S., Parton, A., Blinkhorn, J., Drake, N.A., Jennings, R., Cuthbertson, P., Omari, A. Al, Alsharekh, A.M., Petraglia, M.D., 2018a. The expansion of later Acheulean hominins into the Arabian Peninsula. Scientific Reports. 8, 17165.

Scerri, E.M.L., Thomas, M.G., Manica, A., Gunz, P., Stock, J.T., Stringer, C., Grove, M., Groucutt, H.S., Timmermann, A., Rightmire, G.P., D'Errico, F., Tryon, C.A., Drake, N.A., Brooks, A.S., Dennell, R.W., Durbin, R., Henn, B.M., Lee-Thorp, J., DeMenocal, P., Petraglia, M.D., Thompson, J.C., Scally, A., Chikhi, L., 2018b. Did Our Species Evolve in Subdivided Populations across Africa, and Why Does It Matter? Trends in Ecology & Evolution. 33, 582–594.

Sharp, W.D., Paces, J.B., 2018. Comment on "The earliest modern humans outside Africa." Science.

362, eaat6598.

Shea, J.J., 2008. Transitions or turnovers? Climatically-forced extinctions of Homo sapiens and Neanderthals in the east Mediterranean Levant. Quaternary Science Reviews. 27, 2253–2270.

Scholz, D., Tolzmann, J., Hoffmann, D.L., Jochum, K.P., Spötl, C., Riechelmann, D.F.C., 2014. Diagenesis of speleothems and its effects on the accuracy of ^{230}Th/U-ages. Chemical Geology. 387, 74-86.

Shultz, S., Maslin, M., 2013. Early Human Speciation, Brain Expansion and Dispersal Influenced by African Climate Pulses. PLoS ONE. 8.

Stimpson, C.M., Lister, A., Parton, A., Clark-Balzan, L., Breeze, P.S., Drake, N.A., Groucutt, H.S., Jennings, R., Scerri, E.M.L., White, T.S., Zahir, M., Duval, M., Grün, R., Al-Omari, A., Al Murayyi, K.S.M., Zalmout, I.S., Mufarreh, Y.A., Memesh, A.M., Petraglia, M.D., 2016. Middle Pleistocene vertebrate fossils from the Nefud Desert, Saudi Arabia: Implications for biogeography and palaeoecology. Quaternary Science Reviews. 143, 13–36.

Thomas, H., Geraads, D., Janjou, D., Vaslet, D., Memesh, A., Billiou, D., Bocherens, H., Dobigny, G., Eisenmann, V., Gayet, M., Lapparent de Broin, F., Petter, G., Halawani, M., 1998. First Pleistocene faunas from the Arabian peninsula: an Nafud desert, Saudi Arabia. Comptes Rendus de l'Académie des Sciences - Series IIA - Earth and Planetary Science. 326, 145–152.

Tierney, J.E., deMenocal, P.B., Zander, P.D., 2017. A climatic context for the out-of-Africa migration. Geology. 45, 1023–1026.

Timmermann, A., Friedrich, T., 2016. Late Pleistocene climate drivers of early human migration. Nature. 538, 92–95.

Torfstein, A., Goldstein, S.L., Kushnir, Y., Enzel, Y., Haug, G., Stein, M., 2015. Dead Sea drawdown and monsoonal impacts in the Levant during the last interglacial. Earth and Planetary Science

Letters. 412, 235–244.

Tzedakis, P.C., Crucifix, M., Mitsui, T., Wolff, E.W., 2017. A simple rule to determine which insolation cycles lead to interglacials. Nature. 542, 427–432.

Vaks, A., Bar-Matthews, M., Ayalon, A., Matthews, A., Frumkin, A., Dayan, U., Halicz, L., Almogi-Labin, A., Schilman, B., 2006. Paleoclimate and location of the border between Mediterranean climate region and the Saharo–Arabian Desest as revealed by speleothems from the northern Negev Desert, Israel. Earth and Planetary Science Letters. 249, 384-399.

Vaks, A., Bar-Matthews, M., Ayalon, A., Matthews, A., Frumkin, A. 2018. Pliocene-Pleistocene palaeoclimate reconstruction from Ashalim Cave speleothems, Negev Desert, Israel. Geological Society Special Publications. 446, 201-216.

Vaks, A., Bar-Matthews, M., Matthews, A., Ayalon, A., Frumkin, A., 2010. Middle-Late Quaternary paleoclimate of northern margins of the Saharan-Arabian Desert: Reconstruction from speleothems of Negev Desert, Israel. Quaternary Science Reviews. 29, 2647–2662.

Vaks, A., Woodhead, J., Bar-Matthews, M., Ayalon, A., Cliff, R.A., Zilberman, T, Matthews, A., Frumkin, A., 2013. Pliocene–Pleistocene climate of the northern margin of the Saharo–Arabian Desert recorded in speleothems from the Negev Desert, Israel. Earth and Planetary Science Letters. 368, 88–100.

Wade, L. 2019. Was our species in Europe 210,000 years ago? Science. 365, 111.

Waldmann, N., Torfstein, A., Stein, M., 2010. Northward intrusions of low- and mid-latitude storms across the Saharo-Arabian belt during past interglacials. Geology. 38, 567–570.

Weyhenmeyer, C.E., Burns, S.J., Waber, H.N., Aeschbach-Hertig, W., Kipfer, R., Loosli, H.H., Matter, A., 2000. Cool glacial temperatures and changes in moisture source recorded in Oman groundwaters. Science. 287, 842–845.

Weyhenmeyer, C.E., Burns, S.J., Waber, H.N., Macumber, P.G., Matter, A., 2002. Isotope study of moisture sources, recharge areas, and groundwater flow paths within the eastern Batinah coastal plain, Sultanate of Oman. Water Resources Research. 38, 2-1-2–22.

Williams, M.A.J., Duller, G.A.T., Williams, F.M., Woodward, J.C., Macklin, M.G., El Tom, O.A.M., Munro, R.N., El Hajaz, Y., Barrows, T.T., 2015. Causal links between Nile floods and eastern Mediterranean sapropel formation during the past 125 kyr confirmed by OSL and radiocarbon dating of Blue and White Nile sediments. Quaternary Science Reviews. 130, 89–108.

Woodhead, J., Hellstrom, J., Maas, R., Drysdale, R., Zanchetta, G., Devine, P., Taylor, E., 2006. U-Pb geochronology of speleothems by MC-ICPMS. Quaternary Geochronology. 1, 208–221.

Woodhead, J., Hellstrom, J., Pickering, R., Drysdale, R., Paul, B., Bajo, P., 2012. U and Pb variability in older speleothems and strategies for their chronology. Quaternary Geochronology. 14, 105–113.

Zabel, M., Schneider, R.R., Wagner, T., Adegbie, A.T., De Vries, U., Kolonic, S., 2001. Late quaternary climate changes in central Africa as inferred from terrigenous input to the Niger fan. Quaternary Research. 56, 207–217.

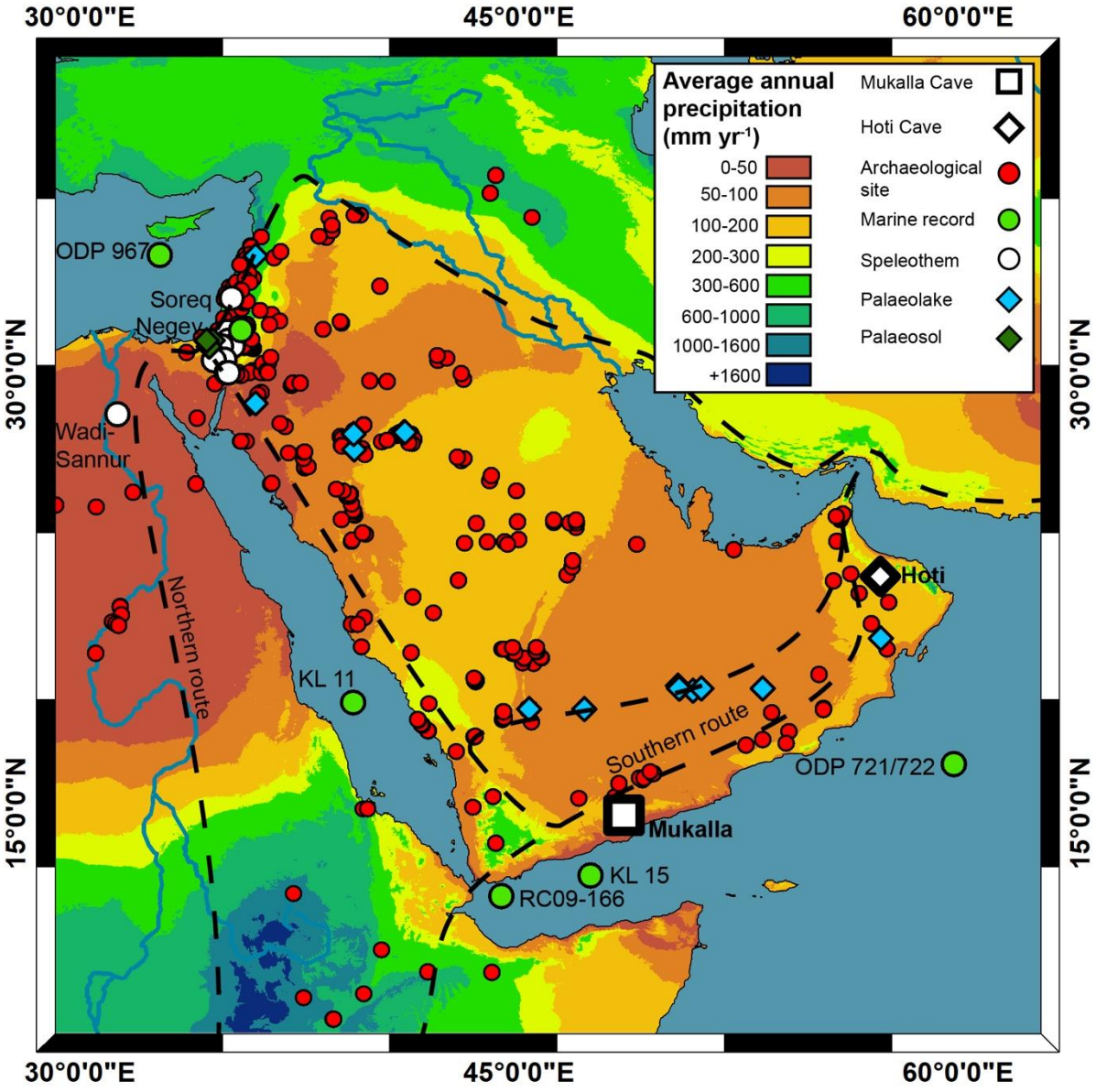

Fig. 1. Map of the Arabian Peninsula with present day (1970-2000) annual precipitation (accessible at: worldclim.org*; Fick and Hijmans, 2017). Red circles denote Middle Palaeolithic archaeological sites (red circles; Bailey et al., 2015; Breeze et al., 2015; Groucutt et al., 2015a, 2015b; Jennings et al., 2015a; Petraglia et al., 2011; Rose et al., 2011). Dashed lines show potential hominin dispersal routes (Rosenberg et al., 2011). Also shown are caves (white cirlces; Bar-Matthews et al., 2003; El-Shenawy et al., 2018; Frumkin et al., 1999; Vaks et al., 2010); palaeolake sites (blue diamonds; Rosenberg et al., 2011, 2012, 2013; Petraglia et al., 2012; Matter et al., 2015), marine records (green circles; deMenocal, 1995; Fleitmann, 1997; Almogi-Labin et al., 2000; Larrasoana et al., 2003; Tierney et al., 2017), lake*

records (blue circles; Torfstein et al., 2015) and Mukalla and Hoti caves (hollow square and diamond, respectively; Burns et al., 1998, 2001; Fleitmann et al., 2003b, 2011).

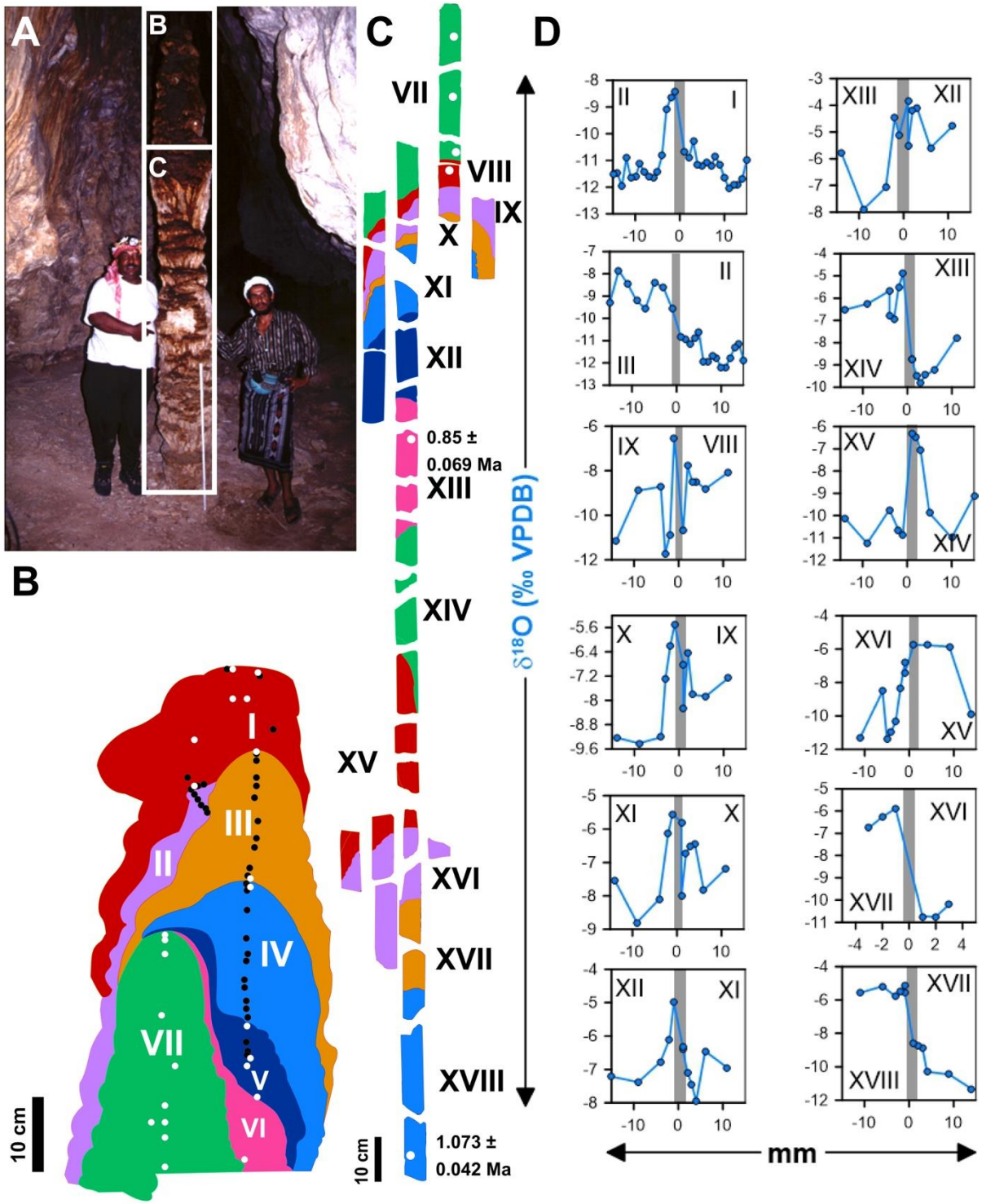

Fig. 2. (A) Stalagmite Y99 in situ in Mukalla Cave. (B and C) Y99 consecutive growth intervals (Fig. S1-S3). Location of ^{230}Th and U-Pb ages marked by black (Fleitmann et al., 2011) and white (this study) circles. (D) Plots show $\delta^{18}O_{ca}$ shifts over discontinuities between GIs (Tab. S6 and S7).

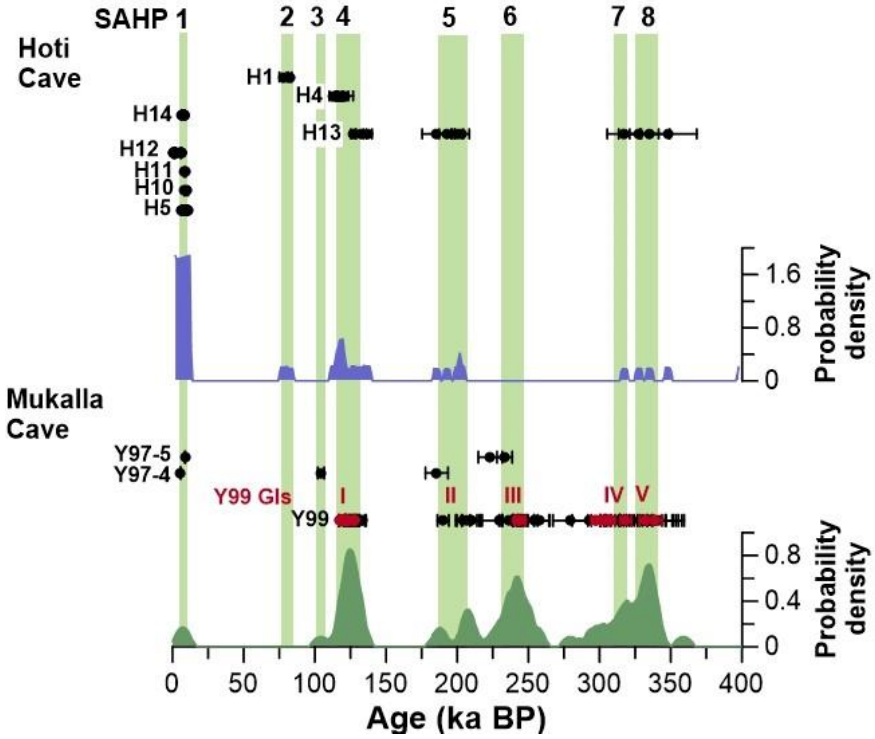

Fig. 3. ^{230}Th ages of Hoti Cave and Mukalla Cave speleothems. Red dots denote new Y99 ^{230}Th ages determined for this study. Age kernel probability density plots of Hoti (blue; 5 pt. moving average) and Mukalla (green) and green bars show periods of most likely speleothem deposition. These were used to assign South Arabian Humid Periods (SAHP) 1-8.

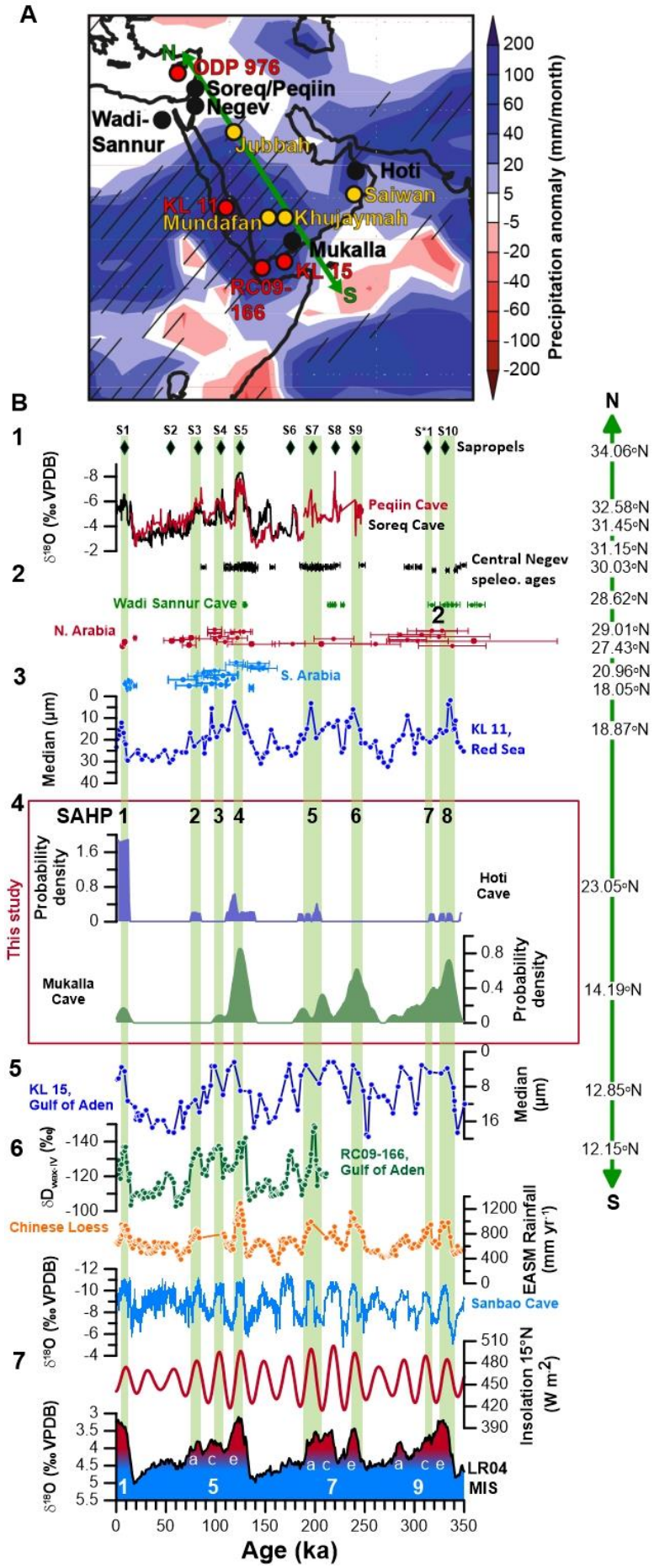
A
N
ODP 976
Soreq/Peqiin
Negev
Wadi-
Sannur
Jubbah
Hoti
Saiwan
KL 11
Mundafan
Khujaymah
Mukalla
KL 15
RC09-
166
S
200
100
60
40
20
5
-5
-20
-40
-60
-100
-200
Precipitation anomaly (mm/month)
B
N
34.06°N
32.58°N
31.45°N
31.15°N
30.03°N
28.62°N
29.01°N
27.43°N
20.96°N
18.05°N
18.87°N
23.05°N
14.19°N
12.85°N
12.15°N
S
S1 S2 S3 S4 S5 S6 S7 S8 S9 S*1 S10
Sapropels
1
δ18O (‰ VPDB)
Peqiin Cave
Soreq Cave
2
Central Negev
speleo. ages
Wadi Sannur Cave
N. Arabia
S. Arabia
3
Median (μm)
KL 11,
Red Sea
4
SAHP 1 2 3 4 5 6 7 8
This study
Probability
density
Hoti
Cave
Mukalla
Cave
5
KL 15,
Gulf of Aden
Median
(μm)
6
δDwax-iV (‰)
RC09-166,
Gulf of Aden
Chinese Loess
EASM Rainfall
(mm yr-1)
Sanbao Cave
7
δ18O (‰ VPDB)
Insolation 15°N
(W m-2)
δ18O (‰ VPDB)
a c e a c e a c e
1 5 7 9
LR04
MIS
Age (ka)

1140

Fig. 4. (A) Location of speleothems (black circles), palaeolakes (yellow circles) and marine sediment cores from the eastern Saharo-Arabian deserts compared to simulated precipitation anomalies (MIS 5e – pre-industrial: Herold and Lohmann, 2009). (1) Sapropel layers in the Eastern Mediterranean Sea (green diamonds; Williams et al., 2015; Grant et al., 2017) vs Peqiin Cave (red) and Soreq Cave (black: Bar-Matthews et al., 2003) $\delta^{18}O$ records; (2) Central Negev (black; Vaks et al. 2010) and Wadi Sannur (green; El-Shenawy et al. 2018) speleothem deposition periods compared to north (red; Petraglia et al., 2012; Rosenberg et al., 2013; Parton et al., 2018) and South Arabian lakes (blue; Rosenberg et al., 2011, 2012; Matter et al., 2015); (3) Red Sea median grain size (Fleitmann, 1997); (4) age kernel density plots of Hoti Cave (blue; 5pt moving average) and Mukalla Cave (green) stalagmites; (5) Gulf of Aden median grain size (Fleitmann, 1997) and $\delta D_{leafwax}$ ‰ (Tierney et al., 2017); (6) Chinese reconstructed rainfall (Beck et al., 2018) vs Sanbao Cave composite speleothem $\delta^{18}O_{ca}$ record (Cheng et al., 2016); (7) Northern hemisphere June insolation at 15°N (Berger and Loutre, 1991, 1999) vs global marine $\delta^{18}O_{benthic}$ (Lisiecki and Raymo, 2005). Marine Isotope Stages follow the taxonomy of Railsback et al. (2015).

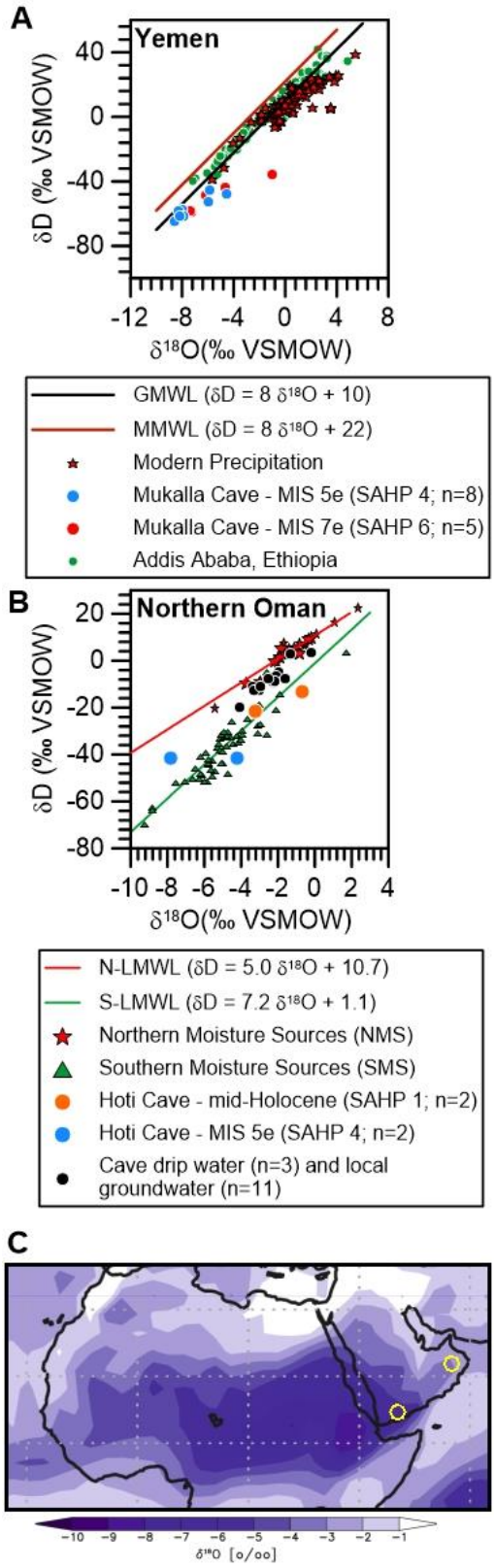

1155

1156 *Fig. 5. Water isotope (δD_{FI} and $\delta^{18}O_{FI}$) values from stalagmites from Mukalla and Hoti Caves (Tab. S9).*

1157 *(A) Stalagmite Y99 δD_{FI} and $\delta^{18}O_{FI}$ values in comparison to δD and $\delta^{18}O$ in modern precipitation in*

1158 *Yemen (Al-ameri et al., 2014) and Ethiopia (IAEA/WMO, 2019. Global Network of Isotopes in*

Precipitation. The GNIP Database. Accessible at: https://nucleus.iaea.org/wiser). Black line denotes the Global Meteoric Waterline (G-MWL: δD = 8 $\delta^{18}O$ + 10). Brown line denotes the Mediterranean Meteoric Waterline (δD = 8 $\delta^{18}O$ + 22) (Gat and Carmi, 1970; Matthews et al., 2000; McGarry et al., 2004). (B) δD_{FI} and $\delta^{18}O_{FI}$ values H5 and H13 compared to regional precipitation values and meteoric waterlines from Northern Oman (N-LMWL: δD = 5.0 $\delta^{18}O$ +10.7; Weyhenmeyer et al., 2000, 2002) and Southern Oman (S-LMWL: δD = 7.2 $\delta^{18}O$ +1.1; Weyhenmeyer et al., 2000, 2002). (C) Locations of Mukalla Cave and Hoti Cave relative to modelled $\delta^{18}O_{precipitation}$ values for boreal summer precipitation during MIS 5e (modified after Herold and Lohmann, 2009). Yellow circles mark the location of Mukalla and Hoti Caves.

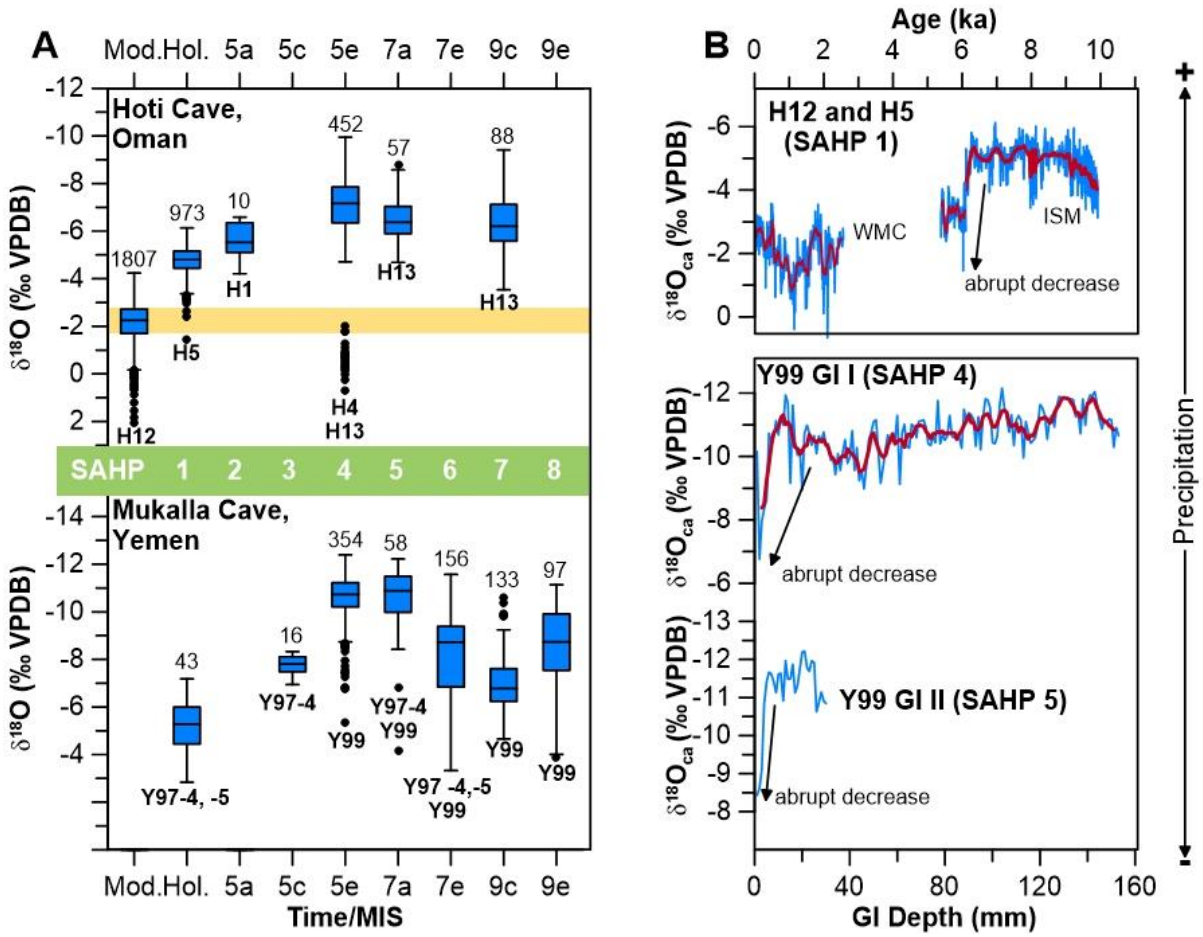

Fig. 6. (A) $\delta^{18}O_{ca}$ whisker-boxplot of Mukalla Cave and Hoti Cave composite records (new Y99 $\delta^{18}O_{ca}$ values combined with data from Fleitmann et al. 2011; Tab. S10). Numbers below whiskers denote

1172 *sample labels and number of $\delta^{18}O_{ca}$ measurements Statistically extreme values marked as black circles.*

1173 *(B) $\delta^{18}O_{ca}$ profiles of Holocene (H5 and H12) and MIS 5e (Y99 GI I) and MIS 7a (Y99 GI II) stalagmites.*

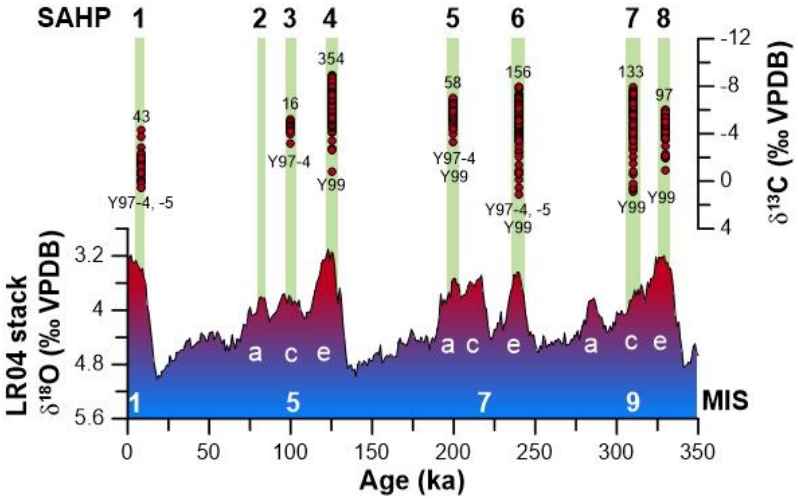

1174

1175 *Fig. 7. $\delta^{13}C_{ca}$ values of Mukalla Cave speleothems during SAHPs I-V (Tab. S11) compared to the LR04*

1176 *stack $\delta^{18}O$ record (Lisiecki and Raymo, 2005).*

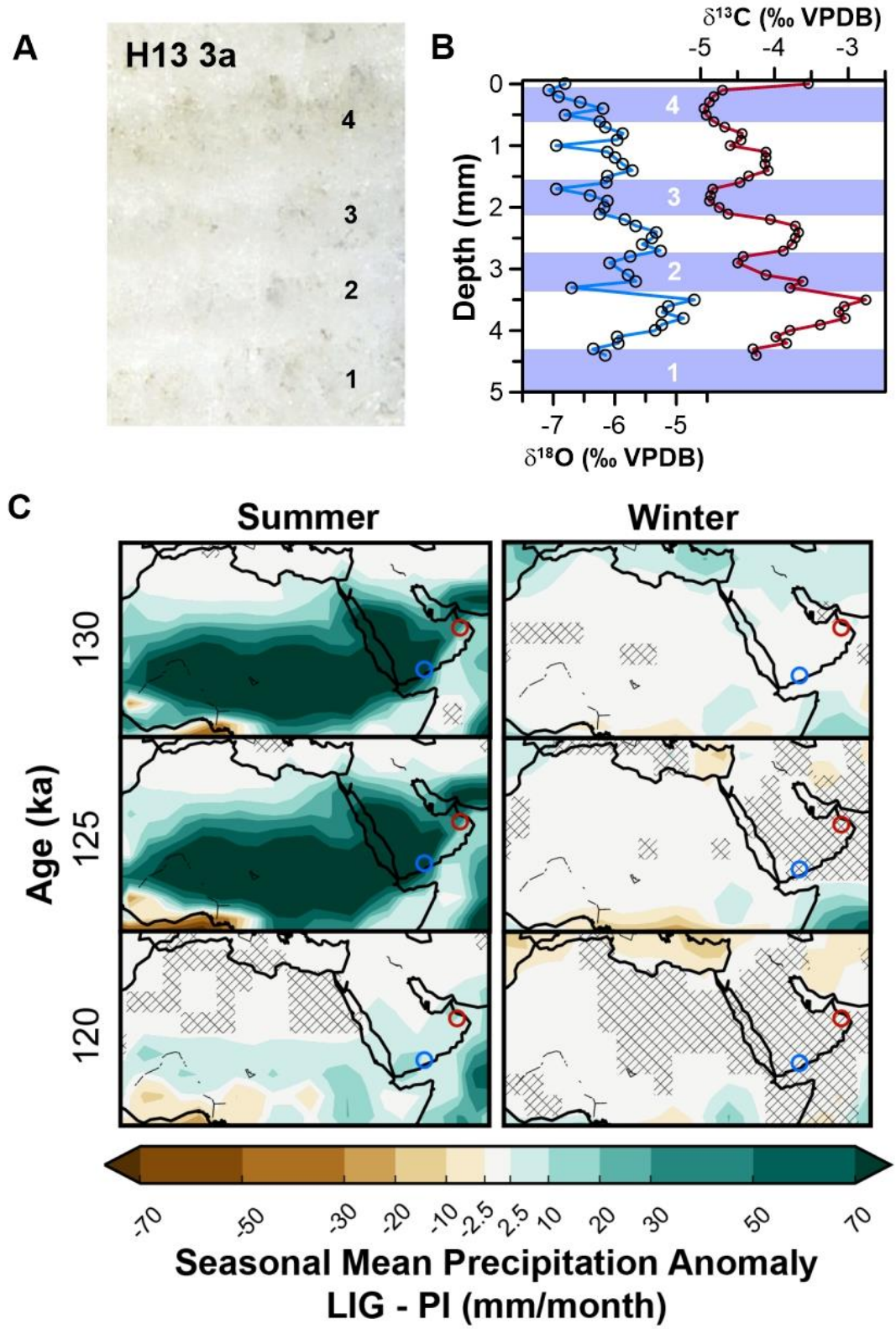
A
H13 3a
4
3
2
1
B
δ13C (‰ VPDB)
-5
-4
-3
0
1
2
3
4
5
Depth (mm)
4
3
2
1
-7
-6
-5
δ18O (‰ VPDB)
C
Summer
Winter
130
125
120
Age (ka)
-70
-50
-30
-20
-10
-2.5
2.5
10
20
30
50
70
Seasonal Mean Precipitation Anomaly
LIG - PI (mm/month)

Fig. 8. (B) Sub-annual $\delta^{18}O_{ca}$ and $\delta^{13}C_{ca}$ values from a MIS 5e section of stalagmite H13 (A) from Hoti Cave (Tab. S8). Shaded blue areas and numbers mark the monsoon seasons. (C) Mukalla Cave (blue circle) and Hoti Cave (red circle) mapped to modelled MIS 5e winter and summer precipitation anomaly (compared to pre-industrial) (Gierz et al., 2017).

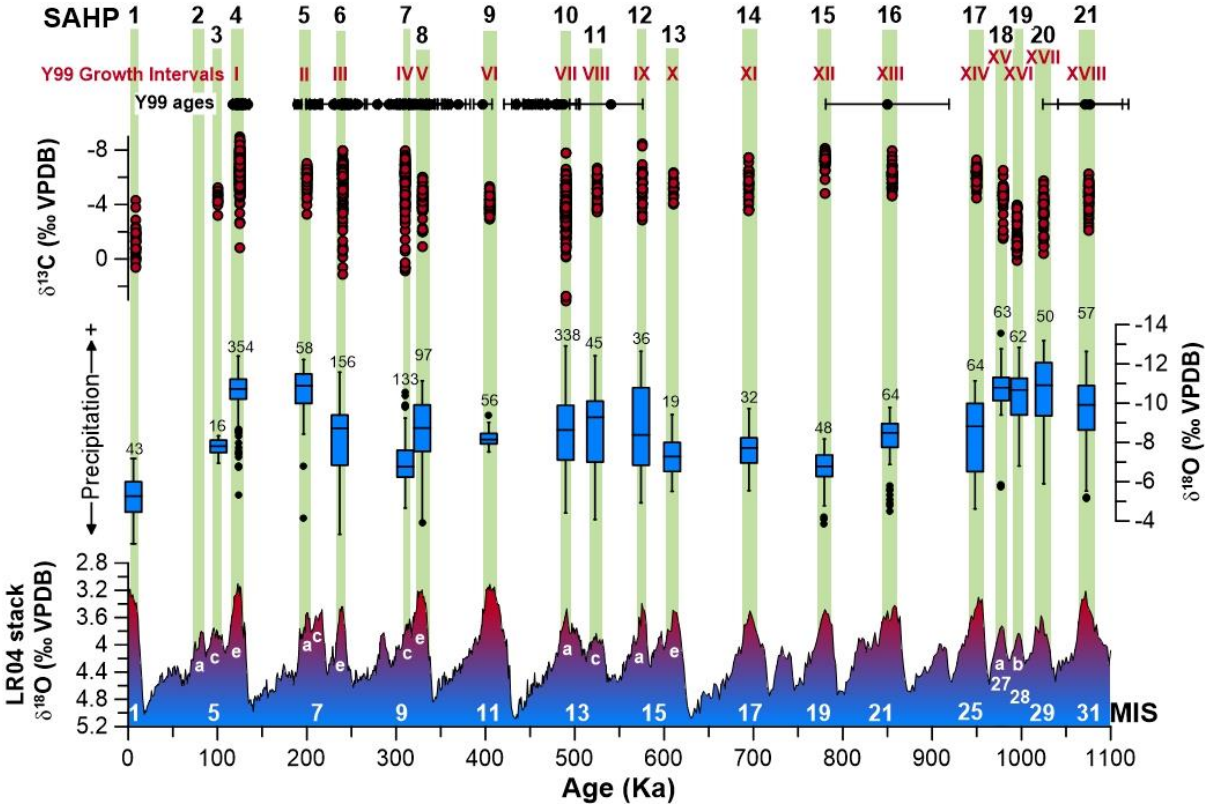

Fig. 9. ^{230}Th (Tab. S1-S3) and U-Pb (Tab. S4 and S5) ages for stalagmite Y99 compared to the LR04 stack $\delta^{18}O$ record (Lisiecki and Raymo, 2005) and extended $\delta^{18}O_{ca}$ and $\delta^{13}C_{ca}$ records of Mukalla Cave stalagmites (Y97-4, Y97-5 and Y99). Undated Y99 growth intervals were assigned to intermediate interglacials and warm substages. Green bars denote timing of SAHPs (South Arabian Humid Periods). Marine Isotope Stages follow the taxonomy of Railsback et al. (2015).

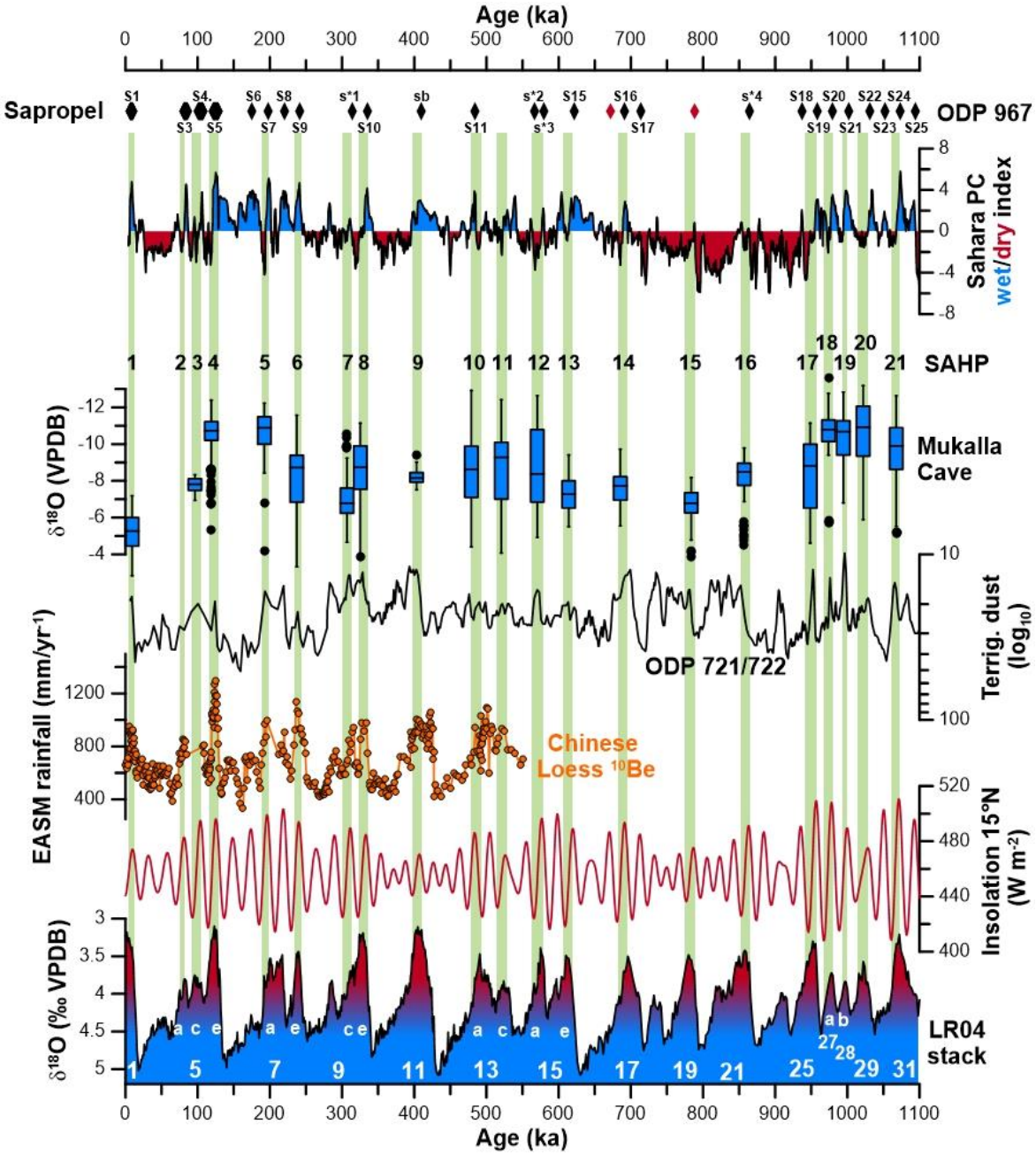

1188

1189 *Fig. 10. SAHPs (green bars) and palaeoclimate records. (Eastern Mediterranean) ODP 967 sapropels*
1190 *(black = identified, red = 'ghost') and wet/dry PCA model (Grant et al., 2017); central Negev desert*
1191 *speleothem ages (Vaks et al., 2010); northern and Southern Arabian palaeolake ages (Rosenberg et*
1192 *al., 2011, 2012, 2013; Matter et al., 2015; Parton et al., 2018) and Mukalla Cave $\delta^{18}O_{ca}$ values; ODP*
1193 *721/722 terrigenous dust (deMenocal, 1995); EASM reconstructed rainfall from Chinese $^{10}Be_{loess}$ (Beck*
1194 *et al., 2018); NHI insolation (W m^{-2}) at 15°N (Berger and Loutre, 1991, 1999) and LR04 stack*

foraminifera $\delta^{18}O_{benthic}$ (Lisiecki and Raymo, 2005) and Marine Isotope Stages following the taxonomy of Railsback et al. (2015).